Quaternary Science Reviews 321 (2023) 108382

Contents lists available at ScienceDirect

Quaternary Science Reviews

journal homepage: www.elsevier.com/locate/quascirev

Revision of the Quaternary calcareous nannofossil biochronology of Arctic Ocean sediments

Mohammad J. Razmjooei [a,b,*], Jorijntje Henderiks [c], Helen K. Coxall [a,b], Karl-Heinz Baumann [d], Flor Vermassen [a,b], Martin Jakobsson [a,b], Frank Niessen [e], Matt O'Regan [a,b,*]

[a] Department of Geological Sciences, Stockholm University, Stockholm, SE-106 91, Sweden
[b] Bolin Centre for Climate Research, Stockholm University, Stockholm, Sweden
[c] Department of Earth Sciences, Uppsala University, Uppsala, SE-752 36, Sweden
[d] Department of Geosciences, University of Bremen, PO Box 330440, 28334, Bremen, Germany
[e] Alfred Wegener Institute, Helmholtz Centre for Polar and Marine Research (AWI), Bremerhaven, Germany

ARTICLE INFO

Handling editor: C. Hillaire-Marcel

Keywords:
Quaternary
Biostratigraphy
Nannoplankton
Arctic ocean
Age-model

ABSTRACT

Despite extensive chronological studies, the relationship between the age and sub-seafloor depth of Arctic Ocean sediments remains ambiguous. This prevents confident identification of paleoceanographic changes in the Arctic during the Quaternary. Currently, age-depth models derived from uranium-series decay in Arctic sediments diverge by hundreds of thousands of years compared to those built on known evolutionary appearances and extinctions of calcareous nannoplankton, a group of globally valuable age-markers. Here we report on high-resolution biostratigraphic analysis of late Quaternary sediments in six cores from the central Arctic Ocean (CAO). We applied paired light microscope (LM) and scanning electron microscope (SEM) imaging to improve nannofossil diagnosis. We argue that low abundances and poor preservation have led to misidentification of the true stratigraphic depth of the critical Pleistocene nannofossil bio-events that have underpinned age models for many Arctic sedimentary records for decades. The revised calcareous nannofossil biochronology provides a radically different geochronological framework for CAO sediments – indicating that what had previously been identified as Marine Isotope Stage (MIS) 7 (191–243 ka) in many sedimentary records is older than MIS 12 (424–478 ka). Furthermore, it suggests that previously inferred sub-stages of MIS 5 could represent full interglacial periods rather than interstadials. The results help reconcile the different dating approaches and provide a transformative step towards resolving the disparity in Quaternary Arctic age-depth models, bringing us one step closer to accurate paleoceanographic reconstructions based on sediment cores.

1. Introduction

Despite more than 50 years of active research, a consensus on the age of Quaternary Arctic Ocean sediments has not been achieved. Numerous dating approaches have been applied in an attempt to constrain the ages, often with very disparate results. Up until the end of the 20th century, paleomagnetic constraints underpinned most age models for Arctic Ocean sediments (Clark, 1970; Spielhagen et al., 1997). However, paleomagnetic interpretations have proven problematic in the Arctic, because, below the first major downhole change in inclination, previously interpreted as the Brunhes-Matuyama reversal event, there is a ubiquitous and thick sequence of high-frequency paleomagnetic excursions for which there is no obvious or unique interpretation (O'Regan et al., 2008). If these polarity changes are interpreted as paleomagnetic chron and subchron boundaries in Lomonosov Ridge sediments, then ages in excess of 5 million years are quickly reached in the upper 8–10 m of sediments (Spielhagen et al., 1997). The ultra-slow sedimentation rates implied by this interpretation contrast starkly to the established Neogene sedimentation rates defined by drilling results from the Integrated Ocean Drilling Program's Expedition 302, which extend further back into the Cenozoic (The Arctic Coring Expedition - ACEX) (Backman et al., 2008) and continues to provide a useful lithostratigraphic reference to which other cores can be compared. At the ACEX drilling site (Fig. 1) an age of ~5 million years was reached between 70 and 80 m below the seafloor, using dinoflagellate cyst biostratigraphy and the exponential decay of $^{10}Be/^{9}Be$ in the recovered sediments (Backman

* Corresponding authors. Department of Geological Sciences, Stockholm University, Stockholm SE-106 91, Sweden.
E-mail addresses: mj.razmjooei@gmail.com (M.J. Razmjooei), matt.oregan@geo.su.se (M. O'Regan).

https://doi.org/10.1016/j.quascirev.2023.108382
Received 19 July 2023; Received in revised form 25 October 2023; Accepted 25 October 2023
Available online 9 November 2023

et al., 2008).

Calcareous nannofossils, like other microfossil groups routinely used for biostratigraphy elsewhere, are scarce in Quaternary Arctic sediments and were not considered in early age models that relied almost exclusively on paleomagnetics. However, identification of the nannofossil species *Emiliania huxleyi* in a sediment core from the Lomonosov Ridge, CAO (96/12-1 PC) transformed age-model interpretations in the Arctic (Jakobsson et al., 2000, 2001) (Fig. 2). The evolutionary first appearance of *E. huxleyi* at ca. 280 ka is a well-established bio-event, globally calibrated to MIS 8 (Thierstein et al., 1977). Evolutionary bio-events can be diachronous at high latitudes due to environmental differences. Studies from the Norwegian Greenland Seas (NGS), where additional oxygen isotope chemostratigraphic age models exist, indicate that *E. huxleyi* entered the NGS Arctic gateway approximately 140 kyrs later, during the MIS 5e interglacial (ca. 120 ka) (Gard and Backman, 1990; Henrich and Baumann, 1994). The application of this MIS 5 age constraint to the *E. huxleyi* occurrence in Core 96/12-1 PC was found to be incompatible with the ages assigned to these sediments (MIS 11–15) using the paleomagnetic-based age model (Spielhagen et al., 1997). This led to a major re-interpretation of the chronology and environmental history of the CAO and the construction of a revised age model in the early 2000's. The new age model implied significantly younger ages and higher sedimentation rates, on the order of 1–2 cm/kyrs for the upper 8–10 m of CAO sediments rather than mm/kyrs (Backman et al., 2004; Spielhagen et al., 2004). This subsequent age model went through various phases of development and testing, including the addition of independent constraints from Optically Stimulated Luminescence (OSL) dating (a geochronological method used to determine the time that has elapsed since certain minerals were last exposed to sunlight or heat) measured on quartz grains (Jakobsson et al., 2003), and has remained central to Arctic chronostratigraphic correlations and paleoceanographic interpretations for two decades (e.g., Jakobsson et al., 2014; Spielhagen et al., 2004; Xiao et al., 2021). It has even been used to derive an 'Arctic specific' age calibration equation for amino acid racemization rates (AAR) in foraminifera (Kaufman et al., 2008) and to age-calibrate appearances of other microfossils, such as the benthic foraminifera *Bulimina aculeata* in CAO sediments (Cronin et al., 2014; Polyak et al., 2013).

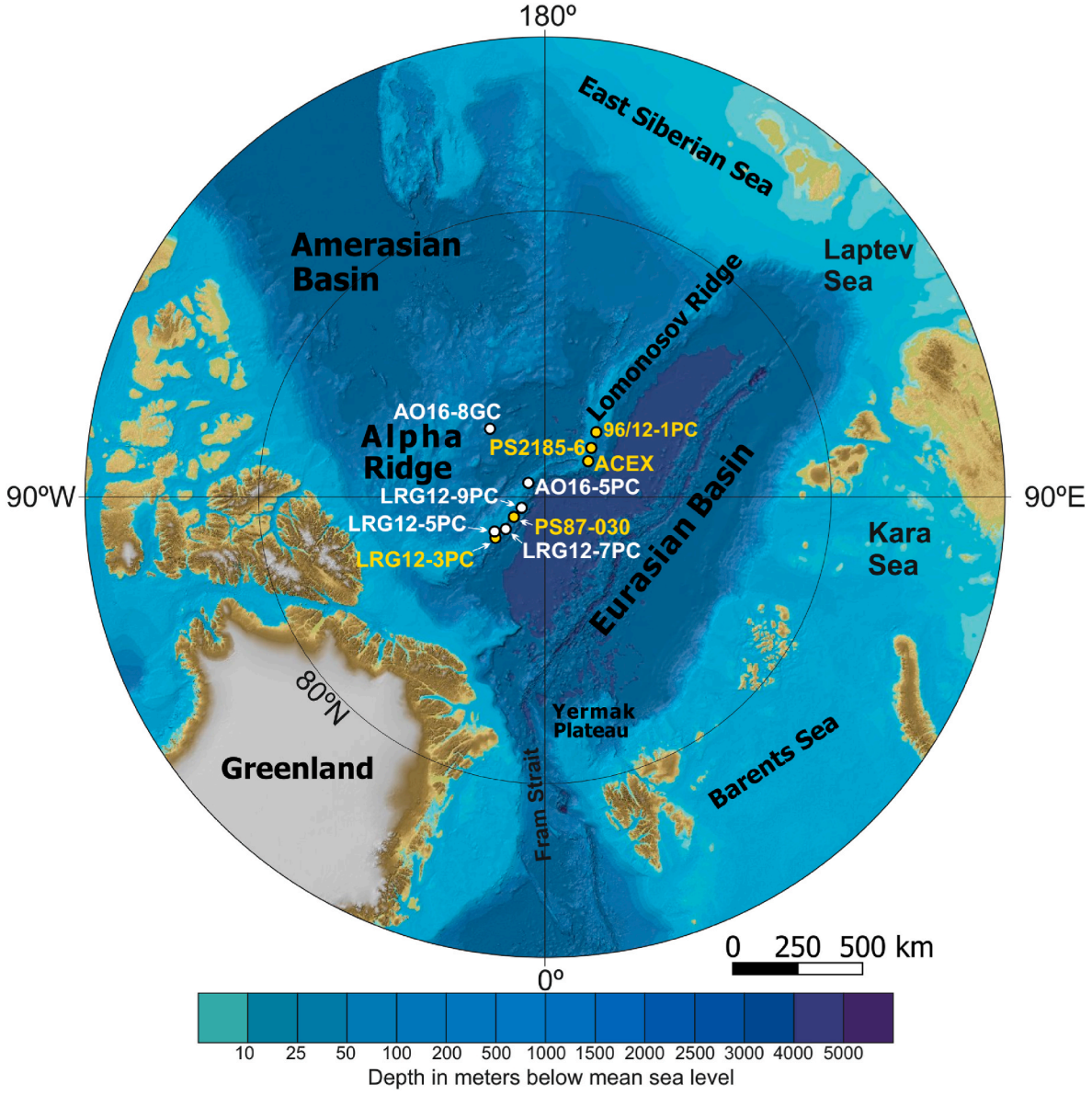

Fig. 1. An overview map of the Arctic Ocean. White dots and labels show the position of the cores that have been studied based on nannofossils for the first time. Yellow dots and labels show the position of cores that have been previously studied by others.

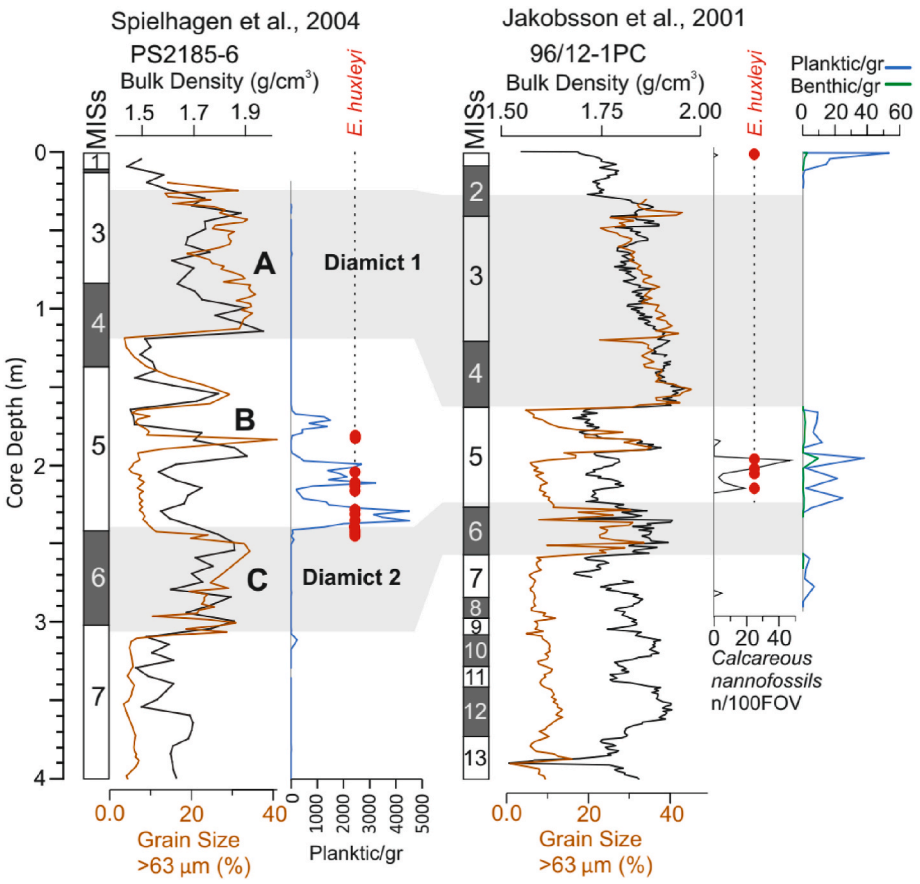

Fig. 2. Stratigraphic correlation between the cores PS2185-6 and 96/12-1 PC based on their grain size and bulk density logs. The abundance of planktic and benthic foraminifera are shown in blue and orange respectively. The previously reported presence of *E. huxleyi* (PS2185-6, Spielhagen et al., 2004, 96/12-1 PC, Jakobsson et al., 2001) are indicated by red dots. The bulk density data of core PS2185-6 are from Bergmann (1996). MISs: Marine Isotope Stages.

A further significant development in the calcareous nannofossil biochronology of CAO sediments was the finding of a second nannofossil bio-event, the last occurrence of *Pseudoemiliania lacunosa* in a sediment core (LRG12-3 PC) from the Lomonosov Ridge (O'Regan et al., 2020). The extinction of *P. lacunosa* occurred globally in MIS 12 (Thierstein et al., 1977), therefore its occurrence in Arctic Ocean sediments provides a minimum age estimate of 424–478 ka (Lisiecki and Raymo, 2005), unless it has been re-deposited from the reworking of older sediments. The identified positions for the FO of *E. huxleyi* and the LO of *P. lacunosa* in LRG12-3 PC (Fig. 1) supported the age models proposed by Jakobsson et al. (2003, 2001, 2000) for the late Quaternary (MIS 1–7) and the longer-term Pleistocene age model developed through cyclostratigraphic analyses of the ACEX record (O'Regan et al., 2008). However, over the past decade there has been increasing discussion about the disparities between the nannofossil-based age model and a third independent chronology derived from the decay of U-series isotopes in sedimentary sequences, which argue again for much lower sedimentation rates (e.g., Not and Hillaire-Marcel, 2012; Geibert et al., 2021; Hillaire-Marcel et al., 2017; Purcell et al., 2022; Song et al., 2023a, 2023b). This family of radiometric age models rely on the decay of ^{230}Th after deposition, and the presence of ^{230}Th that cannot be accounted for by *in-situ* production from the parent ^{234}U, termed $^{230}Th_{excess}$. ^{230}Th has a half-life of ~76 kyrs, therefore excesses of ^{230}Th may be detectable in sediments as old as 300–380 ka (MIS 9–11) (based on 4–5 half-lives). A fundamental discrepancy often arises when these U-series age models are compared to the existing nannofossil stratigraphy of CAO sediments, with the deepest stratigraphic level containing $^{230}Th_{excess}$ occurring above the lowest reported occurrence of *E. huxleyi*. A clear example of this is from PS2185-6, where *E. huxleyi* is reported down to a depth of 245 cm (Spielhagen et al., 2004), but the lowest interval containing $^{230}Th_{excess}$ is at ~170 cm (Purcell et al., 2022). The result is that these two dating approaches result in age models that diverge by multiple glacial cycles for the same sedimentary sequence. Until this discrepancy is resolved, Quaternary paleoceanographic interpretations based on Arctic sediment cores must be viewed in the light that interpreted glacial phases could be wrongly placed in time.

Here we address this problem by examining the calcareous nannofossil biostratigraphy, and provide new observations and interpretations of *P. lacunosa* and *E. huxleyi* distributions from cored sequences in the CAO (Fig. 1). By using paired optical LM and SEM imaging (Gallagher, 1988; Pirini Radrizzani et al., 1990), we find that the low abundance and differing nannofossil preservation state, as well as morphological similarities between some species has generated ambiguities in species-level identification. Based on our new analysis, revised stratigraphic positions are provided for the First Occurrence (FO) of *E. huxleyi* and the Last Occurrence (LO) of *P. lacunosa*. This interpretation of the calcareous nannofossil stratigraphy is a major step towards reconciling disparate age-depth models. It provides a solid foundation for revising Quaternary age models of CAO sediments and the paleoenvironmental interpretations that are based on them.

2. Material and methods

2.1. Marine sediment cores

We have examined the taxonomic composition and abundance of calcareous nannofossil taxa in four cores from the Lomonosov Ridge; LRG12-5 PC, LRG12-7 PC, LRG12-9 PC, AO16-5 PC, and in one core

from the Alpha Ridge; AO16-8 GC (Table 1; Fig. 1; Appendices 1). We also re-examined the calcareous nannofossil taxonomy composition of selected samples from LRG12-3 PC, PS2185-6 and 96/12-1 PC from the Lomonosov Ridge (Table 1; Fig. 1; Appendices 2) that were previously studied by others (Jakobsson et al., 2001; O'Regan et al., 2020; Spielhagen et al., 2004). Uranium (^{234}U, ^{236}U, ^{238}U) and Thorium (^{230}Th, ^{232}Th) isotopic concentrations were measured on samples extracted from cores LRG12-3 PC, LRG12-7 PC, and AO16-5 PC (Appendix 3). Additionally, radiocarbon dating was conducted on four samples extracted from core LRG12-7 PC, and the obtained results were then compared to nannofossil biostratigraphy (see Table 2).

The bulk density records for all the cores in this study were acquired using a Geotek Multi-Sensor-Core-Logger. Measurements on core PS87-030-1 have not been previously published, and were performed on board *RV Polarstern* with the procedure described in Stein (2015).

2.2. Sampling and slide preparation

An initial 10 cm sampling resolution was applied in the top 3–4 m of each core. The sampling resolution was then increased to 5, 3, and 2 cm in fine-grained dark-brown colored units commonly associated with interglacial/interstadial intervals where microfossils tend to be preserved. Higher resolution sampling was undertaken close to biozonal boundaries. Smear slides were prepared from unprocessed sediments and were examined under a polarizing LM at × 1000 and × 1250 magnification. In order to examine the abundance of different taxa, all nannofossils were counted in 100 fields of view (FOV). When the nannofossil abundance was remarkably high, the number of FOVs was reduced to 50 and 20. Additionally, two to three more traverses of each slide were scanned to detect rare and very rare species. The standard NN biozonation scheme (Martini, 1971) was applied based on the selected bio-events.

A settling technique was adopted (Bown and Young, 1998) to obtain good quality slides for SEM analyses and eliminate particles >30 μm and <1 μm. To observe and capture images of the same nannofossil individuals under the LM and SEM, we applied the slide preparation technique proposed by Gallagher (1988) and Pirini Radrizzani et al. (1990) using a copper grid with the coordinate system (e.g., Plate 1). More than 50 microscopic slides and SEM stubs were prepared based on this method from different stratigraphic intervals of cores LRG12-3 PC, LRG12-5 PC, LRG12-7 PC and 96/12-1 PC, and after spending 40 h of SEM observation, a total of 160 images were taken. The success rate of this technique was generally low, as transparent material and debris often partly or entirely covered the surface of the nannofossils (Plates S1–S3). We attempted to overcome this by preparing samples following the filtration technique using membrane filters with 47 mm diameter and 12 μm and 0.8 μm pore size. In many cases, the slides' quality or the preservation of the targeted specimens was still not good enough for clear imaging. In general, the chance of finding a well-preserved specimen using this method was approximately 20%.

Table 1
Locations (Latitude and Longitude), water depths (WD) and length of the cores.

Lat. (°N)	Lon. (°E)	Core	WD(m)	Length(m)
87.098	144.773	96/12-1 PC	1003	7.81
87.531	144.381	PS2185-6	1051	7.68
87.857	136.987	ACEX	1269	428
89.078	−130.547	AO16-5 PC	1253	6.16
86.7795	−140.6433	AO16-8 GC	2620	3.59
89.02672	−73.73444	LRG12-9 PC	1318	6.48
88.6620	−61.5420	PS87-030-1	1277	6.22
88.19764	−55.68453	LRG12-7 PC	2522	6.8
87.82056	−59.63194	LRG12-5 PC	1321	6.29
87.72472	−54.42528	LRG12-3 PC	1607	3.73

Table 2
Radiocarbon dating results from LRG12-7 PC.

LRG12-7 PC	interval (cm)	Lab. Code	Uncalibrated 14C Age (years)	Error
O'Regan et al., 2019	2.5	Beta 457945	5360	30
this study	5–6	OS-171380	9290	30
this study	12–13	OS-171381	31000	490
this study	14–15	OS-171382	31600	530
O'Regan et al., 2019	17	Beta 457946	38780	300
this study	18–19	OS-171383	34100	720
O'Regan et al., 2019	32.5	Beta 457948	42590	460

2.3. U–Th isotopes

Samples were freeze-dried and ground in a pestle and mortar before being sent to an external laboratory (ALS Scientific) for analysis. There, the freeze-dried material was prepared using alkali fusion and measurements were performed using an MC-ICP-MS (NEPTUNE PLUS, ThermoScientific) and ICP-SFMS (ELEMENT2) with internal standardization and external calibration with bracketing isotope standard reference materials. Uncertainties in ^{232}Th and ^{238}U concentrations are less than 5% Relative Standard Deviation (RSD), while the typical uncertainties in ^{232}Th/^{230}Th and ^{238}U/^{234}U ratios are less than 0.5% RSD. ^{230}Th$_{excess}$ was determined by subtracting the activity of ^{234}U from the ^{230}Th activity following the method outlined by Not and Hillaire-Marcel (2012). Activities (dpm/g) were calculated from measured concentrations using half-lives of 245620 years for ^{234}U, and 75584 years for ^{230}Th (Cheng et al., 2013).

2.4. Radiocarbon dating

Radiocarbon dates were acquired from 4 samples containing 900–1100 specimens of plankton foraminifer *Neogloboquadrina pachyderma* from LRG12-7 PC (Table 2). They were measured at the National Ocean Sciences Accelerated Mass Spectrometer (NOSAMS) Facility, Department of Geology and Geophysics, Woods Hole Oceanographic Institution, Massachusetts, USA.

3. Results

3.1. Lithologic description and correlation

Despite the challenges associated with dating Arctic sediments, the downcore lithologic variability can still be confidently correlated over extensive spatial distances. The upper three to 4 m of all the studied cores consist of repetitive intervals of light yellow to dark grey and brown mud. They are generally dominated by fine-grained material with a few pronounced coarser intervals present. Downcore lithologic changes and depositional intervals can be stratigraphically correlated with high confidence using bulk density, direct measurements of grain size, and/or a series of XRF-derived lithologic proxies (i.e. Mn, Zr, Rb, K etc.) (Jakobsson et al., 2001; O'Regan et al., 2019, 2014, 2010; Sellén et al., 2010; Vermassen et al., 2021). The lithostratigraphic correlation, adapted from previous work on these cores (O'Regan et al., 2020, 2019; Vermassen et al., 2021), which can be anchored to the ACEX reference core, is independent of the chronology (Fig. 3).

Broad correlative sedimentary intervals are labeled by capital letters A to E. Intervals D and E are further distinguished by three small coarser grained, tan-colored intervals represented here by small letters a, b and c (α, β, γ in O'Regan et al., 2019) (Figs. S2–S4). Intervals A and C are

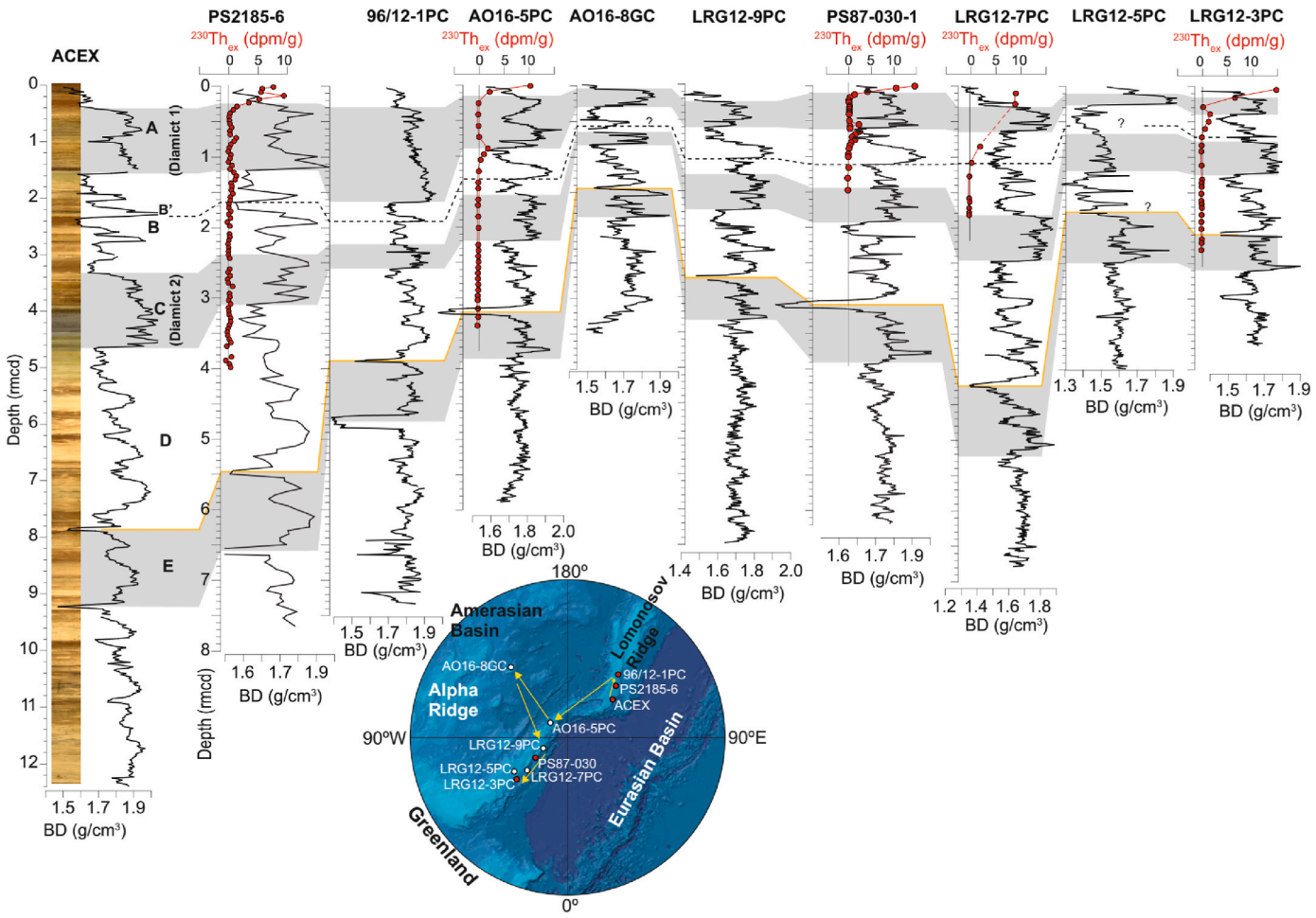

Fig. 3. Stratigraphic correlation of multiple sediment core records from the Lomonosov Ridge and Alpha Ridge illustrated using bulk density (black curves) and $^{230}Th_{excess}$ (red symbols) including the ACEX reference core. Letters A-E identify broad correlative intervals based on the lithologic characteristics. The fine black dashed line shows the base of peak B′, and the fine yellow line indicates a very fine grained (low bulk density) peach colored unit separating intervals D from E. The optimized color image of the ACEX composite record is provided. The ACEX depth scale is the revised meters composite depth (rmcd) published for ACEX (O'Regan et al., 2008). Depths for other cores are reported on simple meters below seafloor (mbsf) scales. The order of the cores from left to right is shown in the small round map. $^{230}Th_{excess}$ data for PS2185-6 are taken from Geibert et al. (2021), those of PS87-030-1 are taken from (Hillaire-Marcel et al., 2017), and the data for AO16-5 PC, LRG12-3 PC and LRG12-7 PC were generated as part of this study (Appendix 3). Bulk Density data of PS87-030-1 are from this study, PS2185-6 are from Bergmann (1996), ACEX from O'Regan et al. (2008), AO16-8 GC from Vermassen et al. (2021), and the remaining data originated by O'Regan et al. (2019).

diamict units (Diamict 1 and Diamict 2 respectively), containing intervals of light to dark grey sediments and variably colored coarse- and fine-grained laminae (O'Regan et al., 2019). The thickness of interval B, located between these diamicts, is highly variable between the coring sites. In many cases, it is further subdivided by an intervening section of one or more thin (ca 10–20 cm thick) coarser grained intervals with relatively high bulk density. The uppermost of these is labeled Peak B'. Peak B′ is positioned just above or coincident with the lowest recorded level of $^{230}Th_{excess}$ and can be correlated across all the cores, but is less clearly defined in LRG12-7 PC, LRG12-5 PC and AO16-8 GC (Fig. 3). In LRG12-3 PC and AO16-5 PC, B′ bracketed by clearly identified pink-to white colored sediments presumably enriched in detrital carbonate. These pink-white layers are very pronounced in sediment cores from the Amerasian Basin (Clark et al., 1980; Polyak et al., 2009; Stein et al., 2010) and are often attributed to iceberg/meltwater discharge events emanating from Paleozoic carbonate bedrock terrains found in the Canadian Arctic Archipelago (Bazhenova et al., 2017; Not and Hillaire-Marcel, 2012), but also extending to the northern margin of Greenland (i.e., O'Regan et al., 2021). These pink-white layers may serve as basin-wide stratigraphic markers, but are not clearly recognized in sediments surrounding B′ in all the cores studied here. Within the stratigraphic framework presented in Fig. 3, the most recently published work on the calcareous nannofossil assemblages in LRG12-3 PC placed the FO of *E. huxleyi* below interval C (Diamict 2), with the LO of *P. lacunosa* at the transition from interval D to E (O'Regan et al., 2020) (Fig. 4 and S6).

3.2. Calcareous nannofossil assemblages

Generally, the preservation of calcareous nannofossils ranges from moderate to poor in all intervals and cores. A total of 14 Quaternary species, including *Emiliania huxleyi*, *Coccolithus pelagicus*, *Calcidiscus leptoporus*, *Gephyrocapsa caribbeanica*, *Gephyrocapsa muellerae*, *Gephyrocapsa oceanica*, *Gephyrocapsa protohuxleyi*, *Pseudoemiliania lacunosa*, *Syracosphaera pulchra*, *Umbilicosphaera* cf. *U. foliosa*, *Reticulofenestra* cf. *R. asanoi*, *Reticulofenestra* sp., *Helicosphaera* cf. *H. carteri*, *Pontosphaera multipora*, and small *Gephyrocapsa* (<2 μm) were identified (Appendix 1; Figs. S1–S5, Plates 1, S1–S7). By considering the birefringence and rim size under the LM, we divided *E. huxleyi* into four different types, including the form with a thick inner cycle and a thick outer cycle herein called *E. huxleyi* TT, the form with a thick inner cycle and a narrow outer cycle called *E. huxleyi* TN, *E. huxleyi* with a narrow inner cycle and a thick outer cycle called *E. huxleyi* NT, and *E. huxleyi* with a narrow inner cycle and a narrow outer cycle called *E. huxleyi* NN (Plates 1 and S1).

Gephyrocapsa caribbeanica and *G. muellerae* were distinguished based on the presence of a high bridge angle to the short axis, an open central area in *G. muellerae*, and an almost closed central area in *G. caribbeanica* and an intermediate bridge angle to the short axis (e.g., Plate S2E and Plate S3A). Occurrences of small (2–3 μm) and large forms (>3 μm) of *G. caribbeanica* and *G. muellerae* were recorded in different categories (*G. caribbeanica* small and *G. muellerae* small) (e.g., Plate S2G, I and J). For those forms of small *Gephyrocapsa* with a thick and high-birefringence bridge we used the term *Gephyrocapsa* HBB (Appendix 1; Plate S2D). We also observed many single-ring coccoliths scattered in

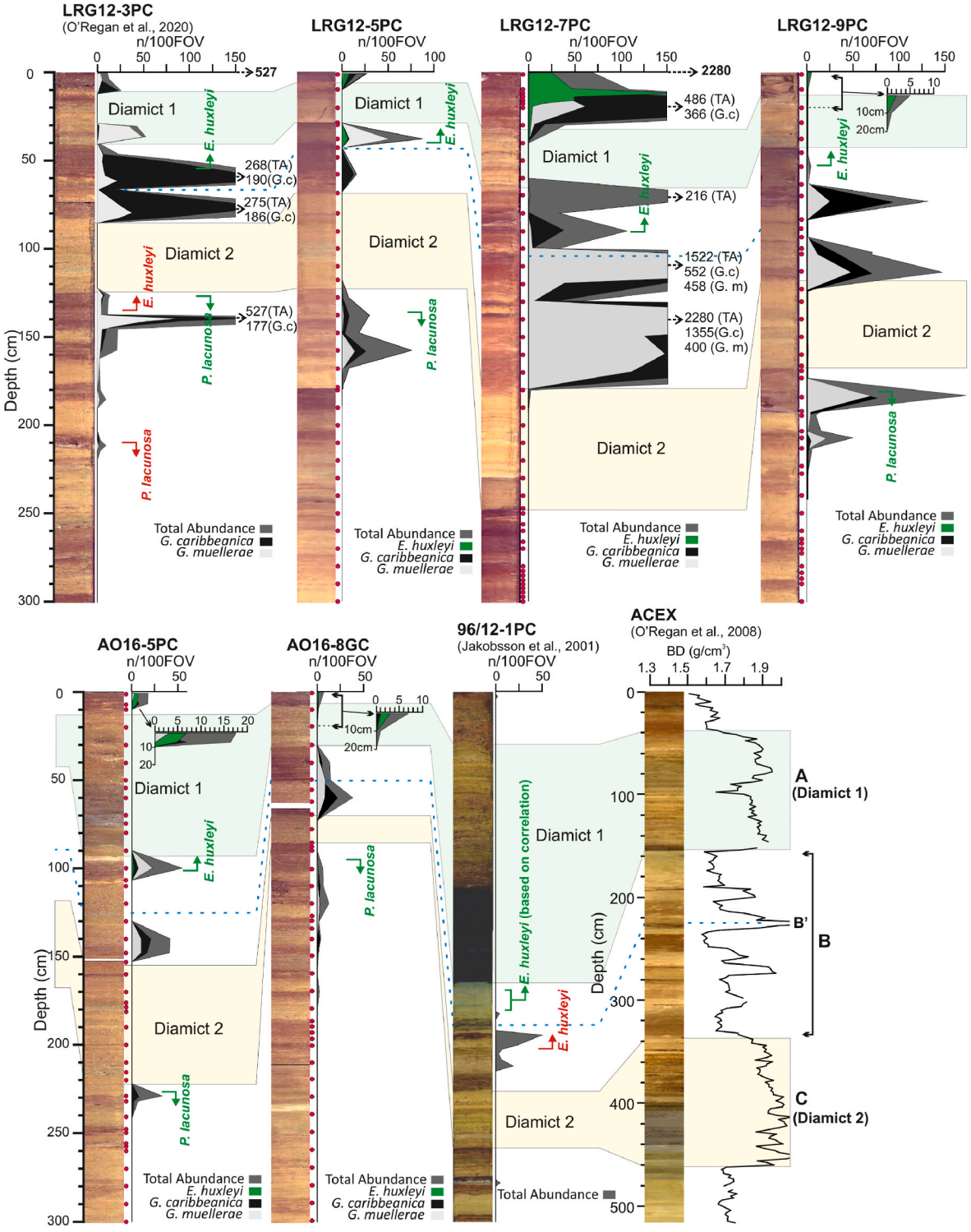

Fig. 4. Stratigraphic correlation between the studied cores (in optimized color) based on the presence of two diamict intervals (following Fig. 3) and the main calcareous nannofossil bio-events. The total abundance and the abundance of some individual calcareous nannofossil assemblages are represented. The red dots show the position of the studied samples in each core. The red arrows in core LRG12-3 PC and 96/12-1 PC indicate the previous biostratigraphic interpretation of O'Regan et al. (2020) and Jakobsson et al. (2001), and the green arrows represent the stratigraphic position of the same bio-events based on this study. The light-green band represents interval A (Diamict 1), the pale-yellow band corresponds to interval C (Diamict 2), and the blue dashed line indicates the location of peak B'. TA: total abundance; G.c: *Gephyrocapsa caribbeanica*; G.m: *Gephyrocapsa muellerae*.

the slides that could belong to any kind of poorly preserved *Gephyrocapsa* or *E. huxleyi* (Plates S1 and S2). We used the abbreviation STR for the specimens with single thick rims and SNR for those with single narrow rims (Appendix 1; Plate S1 and S2). Furthermore, a few reworked species, mostly Late Cretaceous taxa such as *Watznaueria* spp., *Prediscosphaera cretacea*, *Tranolithus orionatus*, and *Micula staurophora*, were documented (Appendix 1; Figs. S2–S5).

Nannofossil abundance is lowest in core AO16-8 GC from the Alpha Ridge and ranges between 1 and 40 specimens per 100 FOV(Fig. 4 and S5; Appendix 1). Abundances are higher but variable in cores from the Lomonosov Ridge, with between 6 and 55 specimens in AO16-5 PC, 1 to 173 specimens in LRG12-9 PC, 30 to 2285 specimens in LRG12-7 PC and 1 to 87 specimens per 100 FOV in LRG12-5 PC (Appendix 1; Fig. 4, S1-S4). Calcareous nannofossils show discontinuous and pulsed occurrences through the upper 1.5–2.5 m of the studied cores but disappear further downcore. They mainly occur in dark brown intervals of finer grain size (lower bulk density) that are commonly associated with bioturbated, microfossil-bearing sediments in the CAO.

The highest number of *E. huxleyi* occurs above interval A (Diamict 1) in all cores, with between 2 and 164 specimens per 100 FOV (Fig. 4). The FO of *E. huxleyi* is confidently found in interval B, between interval A and peak B'. This is the case in all cores except AO16-8 GC, where *E. huxleyi* is only found above interval A, possibly due to the low abundance of nannofossils in this core. Paired LM and SEM imaging illustrates the state of preservation, and in one case (LRG12-5 PC) it shows the existence of *E. huxleyi* below interval A (Plate 1D). Although we anticipated finding *E. huxleyi* between peak B′ and interval C, where it had previously been identified in LRG12-3 PC (O'Regan et al., 2020), PS2185-6 (Spielhagen et al., 2004) and 96/12-1 PC (Jakobsson et al., 2001) (Fig. 2), this was not the case. This zone contained a high number of *G. caribbeanica* and small *Gephyrocapsa* as well as numerous forms including single-ring coccoliths that very closely resemble *E. huxleyi* under the LM (Appendices 1 and 2; Plates 1, S1 and S2). Paired LM and SEM observations illustrate that these *E. huxleyi*-like forms are poorly preserved gephyrocapsid specimens (e.g., Plates 1E-G and S1C-D).

In ACEX, good to moderately preserved specimens of *E. huxleyi*, as well as other coccoliths such as *Gephyrocapsa* spp., were only reported in the first 35 cm above interval A, whereas below this interval, most of the samples were either barren or contained rare and poorly preserved coccoliths (Backman et al., 2006).

In all cores except LRG12-7 PC, *P. lacunosa* is found in low abundance (1 per 100 FOV) below interval C (Diamict 2), often in multiple samples (Appendix 1; Fig. 4, S1-S5). We have confirmed its identification and presence using paired LM and SEM observations (e.g., Plate 1; H-J).

3.3. U- and Th-series isotopes

The downcore distribution of $^{230}Th_{excess}$ in the studied cores within the CAO exhibits two distinct larger peaks: one situated above interval A (Diamict 1) and another positioned between interval A and peak B'. Where sample resolution is higher (PS2185-6, PS87-30-1, LRG12-3 PC) there is also a smaller peak in $^{230}Th_{excess}$ within interval A. These peaks correspond to layers characterized by a lower mean grain size and elevated silt-clay content. The highest $^{230}Th_{excess}$ is recorded at the uppermost sections of the cores, measuring approximately 9.128, 14.663, and 10.256 (dpm/g) for LRG12-7 PC, LRG12-3 PC, and AO16-5 PC, respectively. However, since no measurements were made in trigger weight or multi-cores, we cannot ensure that surface sediments were sampled and measured. A notable decay of $^{230}Th_{excess}$ is evident over time, but to first order, peaks in $^{230}Th_{excess}$ are separated by large intervals where it is absent. These observations notably parallel the outcomes derived from cores PS2185-6 (Geibert et al., 2021), PS87-030-1 (Hillaire-Marcel et al., 2017), and other cores from the CAO (Song et al., 2023b) signifying the absence of $^{230}Th_{excess}$ within ice-rafted debris intervals and layers featuring high sand content. The lowest point where $^{230}Th_{excess}$ is evident at or just below peak B′, and based on the stratigraphic correlation between these records, this appears to be broadly consistent across all studied sites (Fig. 5).

4. Biostratigraphic revision of arctic ocean sediments

There are important differences in the stratigraphic positions of the FO of *E. huxleyi* and the LO of *P. lacunosa* identified in this study compared to previous work (Jakobsson et al., 2001; O'Regan et al., 2020; Spielhagen et al., 2004) (Figs. 4 and 6). Our results suggest that what had been identified as large forms of *E. huxleyi* below interval C (Diamict 2) in LRG12-3 PC (O'Regan et al., 2020) are in fact *P. lacunosa* (Figs. 4 and 6). Partly due to the moderate to poor preservation, critical confidence in the identification of *P. lacunosa* was only achieved after performing the SEM analysis where the relative similarity in the size of the distal and proximal shields, the presence of I or T-shaped elements, and the high number of slits make the distinction between *E. huxleyi* and *P. lacunosa* possible (Plate 1).

The global FO of *E. huxleyi* marks the base of NN21/*E. huxleyi* zone in the standard global nannofossil biozonation of the Martini (1971). Here we place this between interval A (Diamict 1) and peak B′, whereas previous work had reported its occurrence between peak B′ and interval C (Diamict 2). We suggest that below B', what had been identified as *E. huxleyi* and assigned to substages of MIS 5, are likely poorly preserved *Gephyrocapsa* or single-ring coccoliths. Diagenetic etching and partial dissolution of gephyrocapsids that can cause these coccoliths to exhibit features very similar to *E. huxleyi* is not a problem unique to the Arctic (Persico et al., 2003), but can certainly deteriorate because of the low overall nannofossil abundance. These poorly preserved forms are visible within all intervals containing coccoliths. Plate 1 illustrates SEM images of some forms of gephyrocapsids in which the radial elements in their shield construction have become similar to the I-shaped elements in *E. huxleyi* because of dissolution and etching. As long as the relatively well-preserved specimens of *E. huxleyi* are present, this issue is not too problematic. However, when these poorly preserved forms are found stratigraphically below the range of *E. huxleyi*, it becomes difficult to distinguish the FO of *E. huxleyi* based solely on LM observations.

The consistent stratigraphic occurrence for the FO of *E. huxleyi* and LO of *P. lacunosa* in all these cores, despite varying water depths and spatial distribution, suggest that their occurrences are not the result of sediment reworking or mixing. As such, their revised placements in the correlative stratigraphy require a re-assessment of the existing age model. However, one of the crucial issues is that the timing of evolutionary appearances and disappearances in the fossil record may likely be different in the Arctic compared to lower latitudes (diachronism), which must be carefully evaluated.

The first global appearance of *Pseudoemiliania* occurred in the late Zanclean at ~4 Ma (Young, 1998), and its LO was in the middle Pleistocene at ca. 440 ka (Thierstein et al., 1977), coinciding with MIS 12 (467-440 ka, Raffi et al., 2006). It marks the top of the NN19/*P. lacunosa* zone and base of the NN20/*G. oceanica* zone (Martini, 1971). This datum is verified by work from the North Atlantic and NGS (Gard, 1988; Henrich and Baumann, 1994), and identified in sediments on the Yermak Plateau (sites 910C and 911A) drilled during Ocean Drilling Program Leg 151 (Sato and Kameo, 1996) where it was dated to MIS 12 (Knies et al., 2009). Since MIS 12 is a glacial period, it is presumed that nannofossils were not present in the central Arctic, as appears common during recent glacial periods (e.g., Gard, 1986). Hence, the LO of *P. lacunosa* in the central Arctic should have occurred earlier, during the interglacial period of MIS 13 (478–533 ka) (O'Regan et al., 2020). The common position for the LO of *P. lacunosa* just below interval C (Diamict 2) strongly suggests that this is not a result of local re-working. Moreover, the convincing stratigraphic correlation of sedimentary units beneath this diamict (throughout interval D) (Figs. 3 and 5) further indicates that the sudden initiation of coarse-grained deposition did not lead to substantial sediment erosion (i.e. that the sediments underlying Diamict 2 are to the first order, the same age at the different the coring

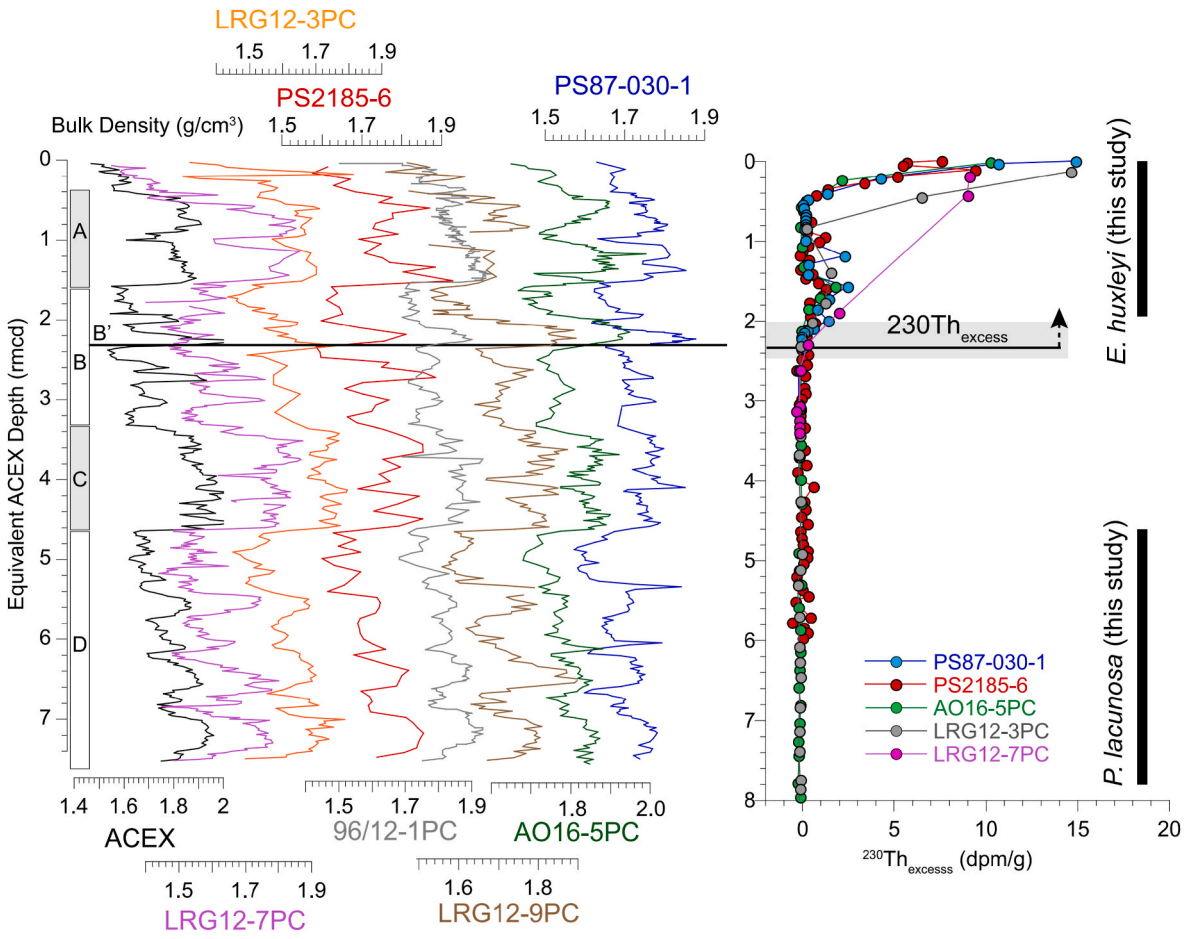

Fig. 5. Stratigraphic correlation of multiple sedimentary cores from the Lomonosov Ridge, displayed on a composite depth scale using bulk density (left) and $^{230}Th_{excess}$ (right). All $^{230}Th_{excess}$ measurements are plotted on the same depth scale. The lowest $^{230}Th_{excess}$ excess in all cores is located near peak B'. The references have been previously provided in the caption for Fig. 3.

sites). While we know that parts of the crest of the Lomonosov Ridge were scoured by glacial ice (Jakobsson et al., 2016), this tended to be in areas shallower than 1000 m water depth, and with mapped areas of ice scouring located quite distant from the coring sites. The occurrence of *P. lacunosa* in sediments beneath interval C indicates that they are older than MIS 12 and likely of MIS 13 age. This is significantly older than the MIS 7 age assigned to this interval in LRG12-3 PC (O'Regan et al., 2020), as well as in PS2185-6 (Spielhagen et al., 2004) and 96/12-1 PC (Jakobsson et al., 2001).

Reticulofenestra asanoi, which has a LO at the boundary of MIS22/MIS 23 (900 ka, Raffi et al., 2006), is a close relative of *P. lacunosa*. Its resemblance to other *Reticulofenestra* specimens, particularly within poorly preserved material, further complicates its accurate recognition. The presence of the form *Reticulofenesta* cf. *R. asanoi*, was noted in some of the cores (Appendix 1). It appears to be sporadic, and there is a significant likelihood that this form may not accurately represent true *R. asanoi*, but rather is either a misidentified *R. asanoi* or potentially a reworked specimen. Therefore, we do not recognize this as a useful or convincing biostratigraphic marker species in these records.

It is widely accepted that *E. huxleyi* evolved during MIS 8 (262–272 ka, Thierstein et al., 1977, 291 ka, Raffi et al., 2006) in both equatorial and subpolar settings. Its abundance remained low for almost 200 kyrs and began to peak in the past 73 kyrs (Thierstein et al., 1977, 63–82 ka, Raffi et al., 2006). Pioneering biostratigraphic studies indicate the first common appearance of *E. huxleyi* during MIS 5 in the NGS (Gard and Backman, 1990; Henrich and Baumann, 1994). The scarcity/absence of *E. huxleyi* before MIS 5 in the NGS has long underpinned arguments for its FO in the Arctic Ocean during MIS 5 (Gard and Backman, 1990; also the results from the Arctic Ocean sediments in Gard, 1993). Recent work adds an additional element of uncertainty, as *E. huxleyi* was identified in the NGS as far back as sediments from MIS 8 age (Sabine-Lamoureux et al., 2022). Further research is required to enhance confidence in the timing of its first appearance in the central Arctic. Clearly, the scarcity of *E. huxleyi* after its evolutionary appearance makes identifying the first occurrence of this species difficult, particularly in the CAO, where the overall abundance of coccoliths is generally very low.

When O'Regan et al. (2020) identified large *E. huxleyi* below interval C in LRG12-3 PC, they were forced to re-assign its FO in the Arctic Ocean to MIS 7, as 1) they were confident of the MIS 5 age for sediments in interval B and 2) because it can be assumed that Arctic sediments would lack nannofossils during MIS 8 due to the presumed intensity of sea-ice cover during glacials. In earlier studies, *E. huxleyi* was identified throughout interval B, and this sequence was entirely assigned to MIS 5 (Jakobsson et al., 2001; O'Regan et al., 2020; Spielhagen et al., 2004) (Fig. 2). However, our new results argue that the FO of *E. huxleyi* is near the top of interval B (above peak B′), and the large *E. huxleyi* reported in O'Regan et al. (2020) below interval C (Diamict 2) are *P. lacunosa* (Figs. 4 and 6). Our quantitative studies reveal that the sediments between peak B′ and the top of interval C, previously argued to be of MIS 5 age, are heavily dominated by *G. caribbeanica* and small *Gephyrocapsa* (Fig. 4). A global dominance of *G. caribbeanica* occurred between MIS 13 to 8 (Bollmann et al., 1998) and also during MIS 7 in co-occurrence with *E. huxleyi* in the North Atlantic (Gard and Backman, 1990). Therefore, the revised placement for the FO of *E. huxleyi* would suggest that the underlying zone dominated by *G. caribbeanica* and small *Gephyrocapsa* was deposited sometime between MIS 13 and MIS 7.

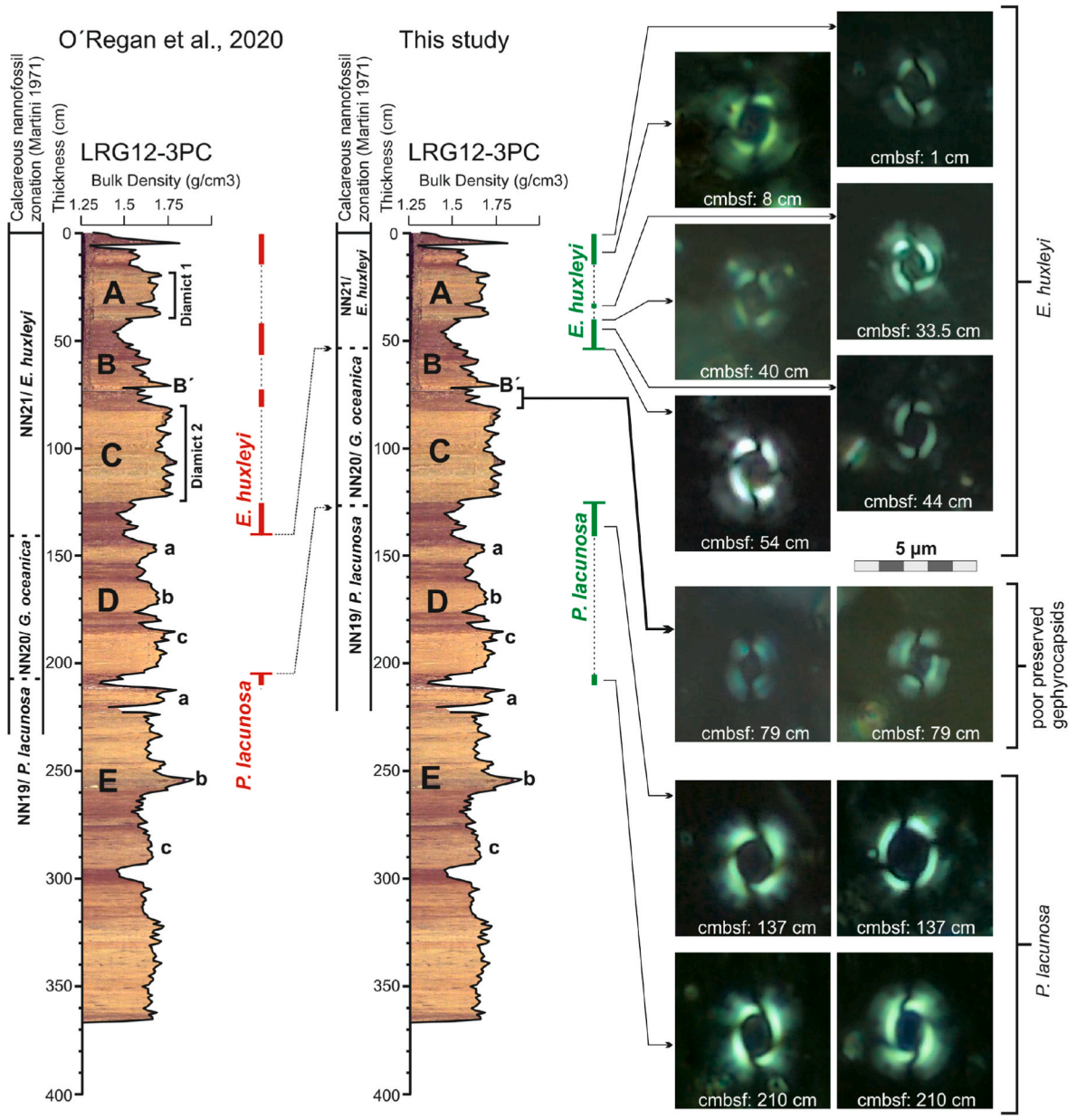

Fig. 6. Core optimized photo and lithology and bulk density of core LRG12-3 PC. The results of biostratigraphic studies by O'Regan et al. (2020) are presented on the left, and the new biostratigraphic results are shown on the right. The red indicates the previous biostratigraphic interpretation, and the green represents the stratigraphic position of the same bio-events based on this study. The scale bar is 5 µm with 1 µm subdivisions.

If the stratigraphic placement for the new FO for *E. huxleyi* is correct, it significantly reduces the disparity between U-series and nannofossil-base age models for CAO sediments. For example, based on the investigation of Hillaire-Marcel et al. (2017) on core PS87-030-1, the extinction of ^{231}Pa excesses, marking a radiometric benchmark age of ~140 ka (near the end of MIS 6), is observed at a depth of 76 cm. This corresponds to the interval between intervals A and peak B′, aligning with the first occurrence of *E. huxleyi* documented in our cores (Figs. 3 and 5). The extinction of ^{230}Th excesses has recently been analysed in a suite of cores from across the CAO (Song et al., 2023b). In PS87-30-1, they estimate an extinction age of 250 ± 18 kyrs at a depth between 109 ± 44 cm, and in PS2185-6, an extinction age of 226 ± 54 kyrs at 174 ± 76 cm (Figs. 2 and 3). Despite the large depth uncertainty attached to these estimates, which arises from the large downcore variability generated by changing environmental and depositional conditions across glacial and interglacial cycles (Song et al., 2023b), these extinction ages suggest that sediments below peak B' are likely MIS 7 or MIS 8 in age. This is consistent with the absence of *E. huxleyi* below this interval, and its widespread occurrence in the central Arctic occurring in MIS 5. Although clearly the uncertainties in both the nannofossil and U-series ages remain large, they now at least overlap.

Another useful biostratigraphic event is the cross-over from higher abundance of *G. caribbeanica* to *E. huxleyi* (*E. huxleyi* acme), first quantified in lower latitudes (Thierstein et al., 1977) where it was correlated within MIS 5b to MIS 5a (~85 ka). However, this cross-over is also time-transgressive (diachronous), and becomes younger with increasing latitude. The same cross-over has been recorded in MIS 4 in sub-polar cores (Thierstein et al., 1977), after MIS 4 in parts of the Nordic Seas (Gard, 1988; Gard and Backman, 1990), and in the upper part of the MIS 3 in radiocarbon dated sediments from the CAO (Backman et al., 2009). Having the advantage of a higher abundance of coccoliths, a thicker sequence of sediments above interval A (Diamict 1) and available radiocarbon dates from planktic foraminifera, the upper 30 cm of core LRG12-7 PC was sampled at 2–3 cm resolution along with four new

radiocarbon measurements (Table 2; Fig. 7). The cross-over between *G. caribbeanica* and *E. huxleyi* in the core occurs between 18 and 16 cm where the abundance of *E. huxleyi* increases from 16 specimens to 49 specimens in 100 FOV, while *G. caribbeanica* abruptly drops from 304 specimens to 35 specimens in 100 FOV. At 12 cm depth in the core, *E. huxleyi* becomes more than the sum of the total abundance of all other species. Radiocarbon dates for the upper 50 cm of core LRG12-7 PC show that the cross-over and the higher abundance of *E. huxleyi* occur between 31 and 34 ^{14}C kyrs (not calibrated due to uncertainties in the local reservoir correction), near the end of MIS 3. This is consistent with the results from Backman et al. (2009) for the Gakkel Ridge and Lomonosov Ridge.

However, two fundamental concerns about the radiocarbon ages in the Arctic Ocean sediments need to be addressed. Firstly, the low sedimentation rates and sediment mixing in the central Arctic Ocean challenge the reliability of ^{14}C-based age-depth inferences (Hillaire-Marcel et al., 2022). However, the core LRG12-7 PC has one of the highest sedimentation rates compared to the other studied cores, with "live" radiocarbon recorded up to ca. 32.5 cm depth. While bioturbation might have mixed Holocene ^{14}C dates to a certain degree, it is unlikely that near-surface dates would be the result of mixing of distinct MIS 1 and MIS 3 populations, especially since bioturbation is usually assumed to affect depth intervals of maximally 10 cm (see Soltwedel et al., 2019).

Secondly, the presence of ^{13}C-enriched authigenic calcite may significantly impact the accuracy of radiocarbon dating and result in older ages and deviations in the chronology of the Arctic Basin sediments (Wollenburg et al., 2023). This means that the crossover between *E. huxleyi* and *G. caribbeanica* might have occurred even later in time, after ca. 31 ^{14}C kyrs (uncalibrated). However, this concern can be partially dismissed because our results are consistent with those from Gakkel Ridge and Lomonosov Ridge (Backman et al., 2009).

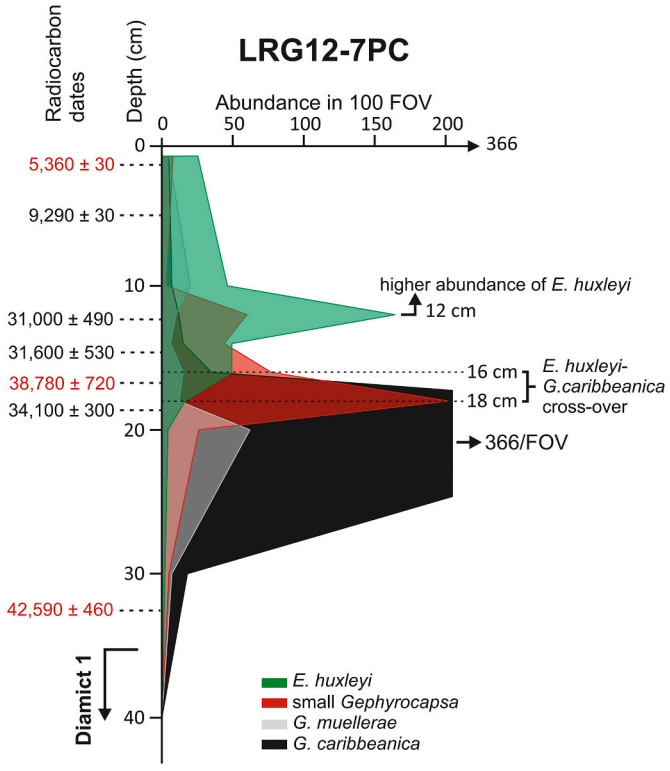

Fig. 7. The stratigraphic cross-over between *G. caribbeanica* (black) and *E. huxleyi* (green) in core LRG12-7 PC. The total abundance (in number per 100 FOV) is also shown for *G. muellerae* (grey) and small *Gephyrocapsa* (red). Radiocarbon dates measured in this study (in black) and those by O'Regan et al. (2019) (in red) are indicated on the left of the depth axis.

5. The global calcareous nannofossil zonation, and the proposed new calibration for calcareous nannofossil zonation for the Arctic Ocean Basin

Since the age of the nannofossil bio-events and biozonal boundaries in the Arctic is different to the standard global calcareous nannofossil event calibrations (e.g., Gartner, 1977; Martini, 1971; Okada and Bukry, 1980), an adapted calibration for the biozonation for the Arctic Ocean Basin is proposed (Fig. 8). The definition of the biozones is derived from the original definitions, and the geological range of each zone is specified for the Arctic Ocean. To characterize biohorizons, the concepts of the "Top Zone" and "Partial Range Zone" from (Wade et al., 2011) are employed to define biozones in the CAO. The prefix 'NN' is borrowed from the nannofossil zonation of Martini (1971) since it has been widely used, and the suffix 'AOB' after the zonal letter refers to the Arctic Ocean Basin.

Name: Zone NN19 AOB/*Pseudoemiliania lacunosa* AOB Top Zone.

Author: Razmjooei et al. (herein).

Definition: Concurrent occurrence of small Gephyrocapsa and *Pseudoemiliania lacunosa* to the last appearance of *Pseudoemiliania lacunosa*.

Reference section: Core LRG12-3 PC

Range: Lower to middle Pleistocene. Unknown MIS to MIS 13.

Remarks: In low latitudes, this zone is defined as the last occurrence of *Discoaster brouweri* to the last appearance of *Pseudoemiliania lacunosa* (Gartner, 1977). However, since *D. brouweri* is not recorded in any of the cores, the base of this zone cannot be defined. Sato and Kameo (1996) similarly reported the absence of this species in the Pliocene records at Yermak Plateau (Sites 910C and 911A) and proposed that the species could be lacking in the Arctic due to a preference for warmer water. The LO of *P. lacunosa* globally occurs coinciding with MIS 12; however, since it is presumed that nannofossils did not inhabit the Arctic during glacial periods due to unfavorable environmental conditions, the LO of *P. lacunosa* is believed to be recorded during the interglacial period of MIS 13 rather than MIS 12 glacial period. Accordingly, the upper portion of the zone aligns closely with Zone NN19 of Martini (1971), although the upper boundary is slightly older in NN19 AOB.

Name: Zone NN20 AOB/*Gephyrocapsa oceanica* AOB Partial Range Zone.

Author: Razmjooei et al. (herein).

Definition: Last appearance of *Pseudoemiliania lacunosa* to the first appearance of *Emiliania huxleyi*.

Reference section: Core LRG12-3 PC

Range: Middle to Upper Pleistocene. From MIS 13 to MIS 5?

Remarks: This zone corresponds to the topmost part of NN19, the whole of NN20 and the lower part of NN21 of (Martini, 1971). The high number of *Gephyrocapsa* (mostly small forms) is noticeable in this interval.

Name: Zone NN21 AOB/*Emiliania huxleyi* AOB Partial Range Zone.

Author: Razmjooei et al. (herein).

Definition: Interval above the first appearance of *Emiliania huxleyi*.

Reference section: Core LRG12-7 PC

Range: Upper Pleistocene to Holocene. From MIS 5? to MIS 1.

Remarks: This zone encompasses the upper portion of zone NN21 of Martini (1971). However, due to the uncertainty surrounding the precise timing of *E. huxleyi*'s initial occurrence in the Arctic, there is doubt associated with the age and the relevant MIS for the lower boundary.

Name: *Emiliania huxleyi* Acme AOB Partial Range Subzone.

Author: Razmjooei et al. (herein).

Definition: Interval above the dominance reversal to *Emiliania huxleyi* from large *Gephyrocapsa* in the Arctic Ocean Basin.

Reference section: Core LRG12-7 PC

Range: Upper Pleistocene to Holocene. From MIS 3 to MIS 1.

Remarks: This zone corresponds to the upper half of zone *E. huxleyi* Acme subzone of Martini (1971).

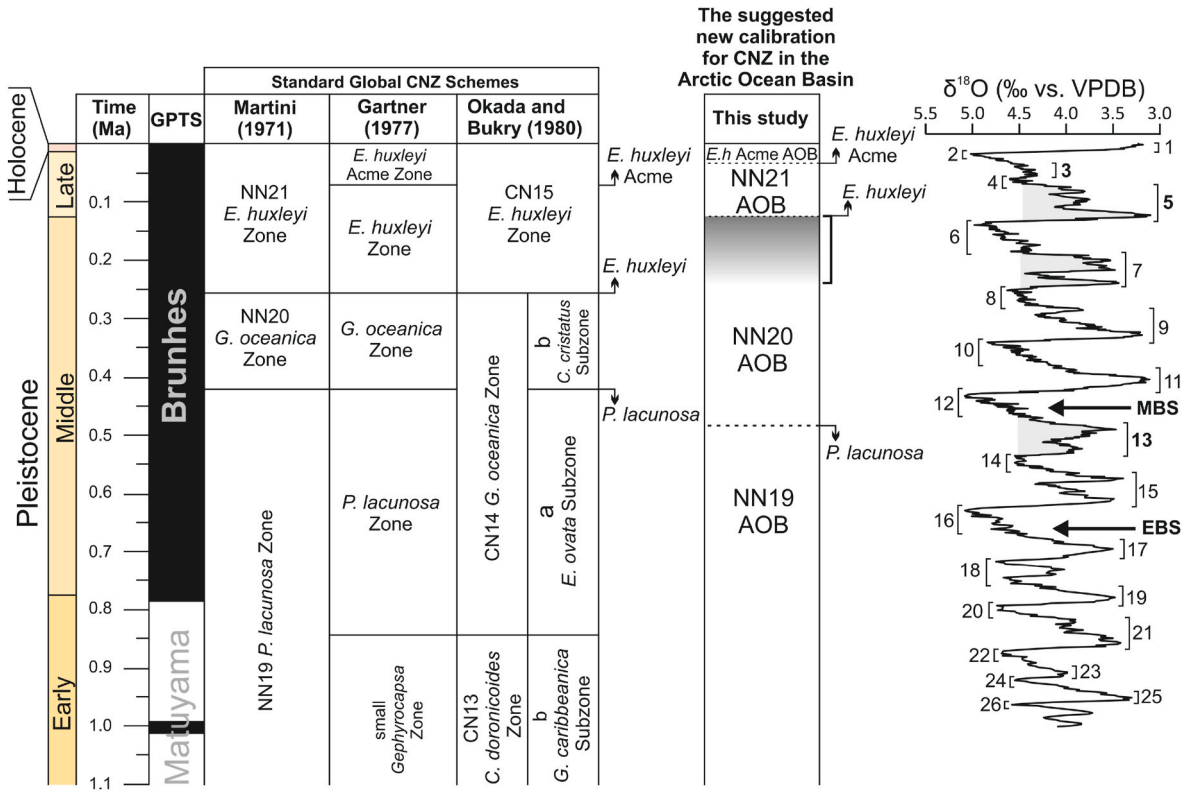

Fig. 8. Comparison of the most important Quaternary nannofossil zonation schemes (after Hine and Weaver, 1998) along with the proposed new time scale for the Arctic Ocean Basin. GPTS: Geomagnetic Polarity Time scale (after Gibbard and Head, 2020). AOB = Arctic Ocean Basin; CNZ = calcareous nannofossil zonation. The marine oxygen isotope stages and substages are shown on the right (after Railsback et al., 2015b). MBS: The Mid-Brunhes Shift to more extreme interglaciation (from Berger and Wefer, 2003). EBS: The Early Brunhes Shift to more extreme glacial (from Railsback et al., 2015a).

6. Discussion and conclusions

In the early 2000's it was the identification using LM observations of *E. huxleyi* in three discrete intervals of core 96/12-1 PC (stratigraphically equivalent to sediments from interval B, Fig. 2) that dramatically changed the accepted age model for CAO sediments (Jakobsson et al., 2000, 2001, 2003). Similar occurrences were confirmed in a nearby core PS2185-6 using SEM (Spielhagen et al., 2004) (Fig. 2). We returned to samples from these two records, and could not confidently identify *E. huxleyi* in the intervals between the two diamict layers using LM and SEM in 96/12-1 PC (Plates S8 and S9) and LM in PS2185-6. Instead, we observed an assemblage dominated by *G. caribbeanica*, *G. muellerae* and small *Gephyrocapsa* as well as many different types of single-ring coccoliths and poorly preserved gephyrocapsids (Plates S8 and S9). Etching and dissolution of nannofossils in these cores may have created structures resembling slits and I-shaped elements in *E. huxleyi*, a critical hypothesis that needs to be explored through more comprehensive SEM analyses.

Hence, our investigation of these five newly acquired records from the CAO reveals a consistent, and considerably different placement for the major nannofossil biozonations in central Arctic sediments. The stratigraphic level that has long been argued to be of MIS 7 age (immediately below Diamict 2) contains *P. lacunosa*, and unless these are all reworked specimens, indicates that these sediments are likely MIS 12 or older. This would significantly alter our understanding of the Arctic's paleoclimate history and suggests the microfossil-bearing intervals between Diamicts 1 and 2 that have long been considered to represent interstadials of MIS 5, could represent multiple late Pleistocene interglacials.

Vermassen et al. (2023) recently reported the widespread occurrence of the subpolar planktonic foraminifera *Turborotalita quinqueloba* throughout interval B in cores from across the inner Arctic, including cores 96/12-1 PC, LRG12-3 PC and AO16-8 GC. They argued that the high abundances and widespread distribution were indicative of a seasonally ice-free Arctic Ocean during the Last Interglacial, based on the existing nannofossil stratigraphy and OSL age model for central Arctic sediments (Fig. 2). Vermassen et al. (2023) identified two peaks in the abundance of *T. quinqueloba* at the base and upper section of interval B. One interpretation that is consistent with the new nannofossil zonations is that the uppermost peak in *T. quinqueloba* abundance occurs in MIS 5(e), while the lowermost peak (in the lower part of interval B) is likely linked to another warm interglacial, most likely associated with MIS 11 (younger than MIS 13). As discussed by Vermassen et al. (2023), proposed U-series ages seem to suggest that the upper peak in subpolar planktonic foraminifer would occur in MIS 7, while the equivalent interval to the base of interval B is either argued to be MIS 13 (see in Hillaire-Marcel and de Vernal, 2022) or not assigned an age due to the complexities of extrapolating the U-series age models beyond extinction ages (Song et al., 2023a, 2023b).

The new time constraints suggested in this study would be partially more consistent with arguments made by proponents of U-series based age models for Quaternary Arctic Ocean sediments (e.g., Geibert et al., 2021; Hillaire-Marcel et al., 2017; Purcell et al., 2022), as well as results from amino acid racemization rates in planktic and benthic foraminifera (West et al., 2022). At the same time, the new nannofossil biozonations are not compatible with results from OSL dating on quartz grains (Jakobsson et al., 2003), which supported an MIS 5 age for sediments throughout interval B, nor with the paleomagnetic-based interpretations that seek to place the Brunhes-Matuyama boundary at the base of Interval C (Diamict 2) which would require a period of severely reduced sedimentation or regional erosion, for which no evidence yet exists. These inconsistencies are now the challenges to overcome in developing revised age models for CAO sediments.

The revised stratigraphic placements for the FO of *E. huxleyi* and LO

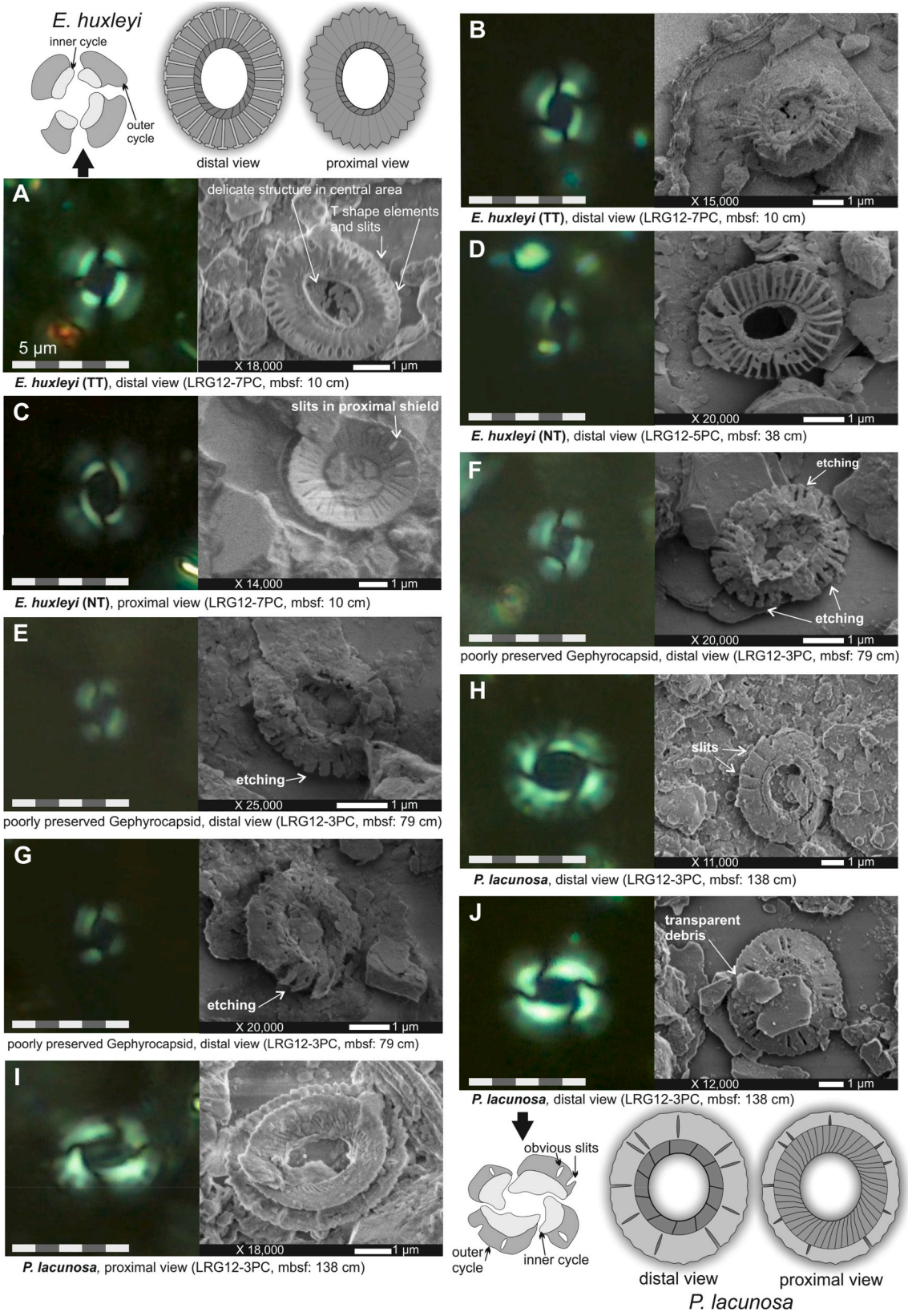

Plate 1. Nannofossil micrographs and schematic illustrations in support of the refined taxonomic identifications central to this study. Optical LM and SEM micrographs of the same individuals of *E. huxleyi* (A–D), poorly preserved gephyrocapsids that resemble *E. huxleyi* under the LM (E–G), and *P. lacunosa* (H–J). All the light microscopy micrographs are taken under cross-polarized light at 1000X magnification. The core name, sample number, and depth are provided. The scale bar for light micrographs is 5 µm divided into five portions, each with 1 µm length. The schematic illustrations of *E. huxleyi* and *P. lacunosa* are based on the specimens in A and J respectively, but are broadly representative of the different taxa.

of *P. lacunosa* indicate that middle to late Pleistocene sedimentation rates are lower than what has been reported in the past, yet still higher than the ultra-low sedimentation rate proposed by early paleomagnetic interpretations (e.g., Clark, 1970; Spielhagen et al., 1997). In this respect, it is important to note the large variability in the thickness of sediments between the two major diamict units (Fig. 3), which range from 170 cm in ACEX to 40 cm in AO16-8 GC and LRG12-3 PC. In expanded sequences such as ACEX, or even LRG12-7 PC (Fig. 3), the interval between the two diamict units exhibits a lot of lithologic variability that cannot be easily correlated to sequences in the more condensed sites (i.e., LRG12-3 PC; LRG12-5 PC; PS87-030-1, AO16-8 GC). These cm-to decimeter thick coarser intervals (recognized by the higher bulk density) are either stadials, full glacials, or local depositional events. How they are interpreted will have a profound impact on the resulting age model if 'cycle-counting' approaches are applied in age model construction – this includes the extrapolation of results or sedimentation rates based on U-series decay. A coherent age model for Quaternary Arctic Ocean sediments should resolve the discrepancies between existing dating approaches, and acknowledge and account for the regional variability in sedimentation rates. As a result of these outstanding challenges, we do not attempt to use the new nannofossil biozonations to identify MIS boundaries. Instead, we present this new scheme as a foundation for further developing geochronological approaches for dating Arctic Ocean sediments and reconciling outstanding disparities between different dating methods.

Author contribution

MJR: Calcareous nannofossils taxonomy and biostratigraphy, interpretation, writing the original draft; MO: supervision, interpretation, writing, reviewing, and editing of the paper; JH and KB: interpretation, reviewing the calcareous nannofossil taxonomy; FN generated and processed the BD data of core PS87/30-1; FV, HKC and MJ and all other co-authors contributed to the writing and final editing of the paper.

Declaration of competing interest

The authors declare that they have no known competing financial interests or personal relationships that could have appeared to influence the work reported in this paper.

Data availability

Data will be made available on request.

Acknowledgment

We would like to extend our gratitude to Professor Hillaire-Marcel, the editor of the QSR journal, and the two anonymous reviewers for their valuable and constructive suggestions. We thank Lilian Geekie for collecting foraminifera shells to conduct radiocarbon dating analyses. Kjell Jansson is thanked for his help with SEM imaging. Jorg Bollmann and Jose Dominick Guballa are thanked for checking calcareous nannofossils in five slides from core LRG12-3 PC. Additional thanks go to the NOSAMS Facility for expeditious dating of the samples. MJR and MO are supported by the Swedish Research Council under Grant DNR-2020–04379 and MJ by Grant 2022-03718. FN was supported by the AWI Research Program 'Cryosphere and Climate' Workpackage 2.1.

Appendix A. Supplementary data

Supplementary data to this article can be found online at https://doi.org/10.1016/j.quascirev.2023.108382.

References

Backman, J., Fornaciari, E., Rio, D., 2009. Biochronology and paleoceanography of late Pleistocene and Holocene calcareous nannofossil abundances across the Arctic Basin. Mar. Micropaleontol. 72, 86–98. https://doi.org/10.1016/j.marmicro.2009.04.001.

Backman, J., Jakobsson, M., Frank, M., Sangiorgi, F., Brinkhuis, H., Stickley, C., O'Regan, M., Løvlie, R., Pälike, H., Spofforth, D., Gattacecca, J., Moran, K., King, J., Heil, C., 2008. Age model and core-seismic integration for the cenozoic arctic coring expedition sediments from the Lomonosov Ridge: ACEX age model. Paleoceanography 23. https://doi.org/10.1029/2007PA001476.

Backman, J., Jakobsson, M., Løvlie, R., Polyak, L., Febo, L.A., 2004. Is the central Arctic Ocean a sediment starved basin? Quat. Sci. Rev. 23, 1435–1454. https://doi.org/10.1016/j.quascirev.2003.12.005.

Integrated Ocean drilling Program. In: Backman, J., Moran, K., McInroy, D.B., Mayer, L. A. (Eds.), 2006. https://doi.org/10.2204/iodp.proc.302.2006.

Bazhenova, E., Fagel, N., Stein, R., 2017. North American origin of "pink–white" layers at the Mendeleev Ridge (Arctic Ocean): new insights from lead and neodymium isotope composition of detrital sediment component. Mar. Geol. 386, 44–55. https://doi.org/10.1016/j.margeo.2017.01.010.

Berger, W.H., Wefer, G., 2003. On the dynamics of the ice ages: Stage-11 Paradox, mid-brunhes climate shift, and 100-ky cycle. In: Droxler, A.W., Poore, R.Z., Burckle, L.H. (Eds.), Geophysical Monograph Series. American Geophysical Union, Washington, D. C., pp. 41–59. https://doi.org/10.1029/137GM04

Bergmann, U., 1996. Physical Properties of Sediment Core PS2185-6. https://doi.org/10.1594/PANGAEA.50137.

Bollmann, J., Baumann, K.-H., Thierstein, H.R., 1998. Global dominance of *Gephyrocapsa* coccoliths in the Late Pleistocene: selective dissolution, evolution, or global environmental change? Paleoceanography 13, 517–529. https://doi.org/10.1029/98PA00610.

Bown, P., Young, J.R., 1998. Techniques. In: Bown, P. (Ed.), Calcareous Nannofossil Biostratigrapgy. British Micropalaeontology Society Publications Series. Kluwer Academic Publisher, Cambridge, pp. 16–28.

Cheng, H., Lawrence Edwards, R., Shen, C.-C., Polyak, V.J., Asmerom, Y., Woodhead, J., Hellstrom, J., Wang, Y., Kong, X., Spötl, C., Wang, X., Calvin Alexander, E., 2013. Improvements in 230Th dating, 230Th and 234U half-life values, and U–Th isotopic measurements by multi-collector inductively coupled plasma mass spectrometry. Earth Planet Sci. Lett. 82–91. https://doi.org/10.1016/j.epsl.2013.04.006, 371–372.

Clark, D.L., 1970. Magnetic reversals and sedimentation rates in the Arctic Basin. Geol. Soc. Am. Bull. 81, 3129–3134. https://doi.org/10.1130/0016-7606(1970)81[3129:MRASRI]2.0.CO;2.

Clark, D.L., Whitman, R.R., Morgan, K.A., Mackey, S.D., 1980. Stratigraphy and Glacial-Marine Sediments of the Amerasian Basin, Central Arctic Ocean, Geological Society of America Special Papers. Geological Society of America. https://doi.org/10.1130/SPE181.

Cronin, T.M., DeNinno, L.H., Polyak, L., Caverly, E.K., Poore, R.Z., Brenner, A., Rodriguez-Lazaro, J., Marzen, R.E., 2014. Quaternary ostracode and foraminiferal biostratigraphy and paleoceanography in the western Arctic Ocean. Mar. Micropaleontol. 111, 118–133. https://doi.org/10.1016/j.marmicro.2014.05.001.

Gallagher, L.T., 1988. A technique for viewing the same nannofossil specimen in light microscope and scanning electron microscope using standard preparation materials. J. Micropalaeontol. 7, 53–57. https://doi.org/10.1144/jm.7.1.53.

Gard, G., 1993. Late Quaternary coccoliths at the North Pole: evidence of ice-free conditions and rapid sedimentation in the central Arctic Ocean. Geology 21, 227. https://doi.org/10.1130/0091-7613(1993)021<0227:LQCATN>2.3.CO;2.

Gard, G., 1988. Late quaternary calcareous nannofossil biozonation, chronology and palaeo-oceanography in areas north of the faeroe-Iceland ridge. Quat. Sci. Rev. 7, 65–78. https://doi.org/10.1016/0277-3791(88)90094-7.

Gard, G., 1986. Calcareous nannofossil biostratigraphy of late Quaternary Arctic sediments. Boreas 15, 217–229. https://doi.org/10.1111/j.1502-3885.1986.tb00926.x.

Gard, G., Backman, J., 1990. Synthesis of arctic and sub-arctic coccolith biochronology and history of North Atlantic drift water influx during the last 500.000 years. In: Geological History of the Polar Oceans: Arctic versus Antarctic. NATO ASI Series, pp. 437–445.

Gartner, S., 1977. Calcareous nannofossil biostratigraphy and revised zonation of the Pleistocene. Mar. Micropaleontol. 2, 1–25. https://doi.org/10.1016/0377-8398(77)90002-0.

Geibert, W., Matthiessen, J., Stimac, I., Wollenburg, J., Stein, R., 2021. Glacial episodes of a freshwater Arctic Ocean covered by a thick ice shelf. Nature 590, 97–102. https://doi.org/10.1038/s41586-021-03186-y.

Gibbard, P.L., Head, M.J., 2020. The quaternary period. In: Geologic Time Scale 2020. Elsevier, pp. 1217–1255. https://doi.org/10.1016/B978-0-12-824360-2.00030-9.

Henrich, R., Baumann, K.-H., 1994. Evolution of the Norwegian Current and the Scandinavian Ice Sheets during the past 2.6 m.y.: evidence from ODP Leg 104 biogenic carbonate and terrigenous records. Palaeogeogr. Palaeoclimatol. Palaeoecol. 108, 75–94. https://doi.org/10.1016/0031-0182(94)90023-X.

Hillaire-Marcel, C., de Vernal, A., 2022. A comment about "A sedimentary record from the Makarov Basin, Arctic Ocean, reveals changing middle to Late Pleistocene glaciation patterns". Quat. Sci. Rev. 270 (2021), 107176 https://doi.org/10.1016/j.quascirev.2021.107239 from W. Xiao, L. Polyak, R. Wang, C. Not, L. Dong, Y. Liu, T. Ma, T. Zhang. Quat. Sci. Rev. 279, 107239.

Hillaire-Marcel, C., de Vernal, A., Rong, Y., Roberge, P., Song, T., 2022. Challenging radiocarbon chronostratigraphies in central Arctic Ocean sediment. Geophys. Res. Lett. 49, e2022GL100446 https://doi.org/10.1029/2022GL100446.

Hillaire-Marcel, C., Ghaleb, B., de Vernal, A., Maccali, J., Cuny, K., Jacobel, A., Le Duc, C., McManus, J., 2017. A new chronology of late quaternary sequences from the

central Arctic Ocean based on "extinction ages" of their excesses in ^{231} Pa and ^{230} Th: late quaternary Arctic Ocean chronology. Geochem. Geophys. Geosystems 18, 4573–4585. https://doi.org/10.1002/2017GC007050.

Hine, N., Weaver, P.P.E., 1998. Quaternary. In: Bown, P. (Ed.), Calcareous Nannofossil Biostratigraphy. British Micropalaeontology Society Publications Series, Cambridge: Kluwer Academic Publisher, pp. 266–283.

Jakobsson, M., Andreassen, K., Bjarnadóttir, L.R., Dove, D., Dowdeswell, J.A., England, J.H., Funder, S., Hogan, K., Ingólfsson, Ó., Jennings, A., Krog Larsen, N., Kirchner, N., Landvik, J.Y., Mayer, L., Mikkelsen, N., Möller, P., Niessen, F., Nilsson, J., O'Regan, M., Polyak, L., Nørgaard-Pedersen, N., Stein, R., 2014. Arctic Ocean glacial history. Quat. Sci. Rev. 92, 40–67. https://doi.org/10.1016/j.quascirev.2013.07.033.

Jakobsson, M., Backman, J., Murray, A., Løvlie, R., 2003. Optically Stimulated Luminescence dating supports central Arctic Ocean cm-scale sedimentation rates: osl-dating of Arctic Ocean sediments. Geochem. Geophys. Geosystems 4. https://doi.org/10.1029/2002GC000423.

Jakobsson, M., Løvlie, R., Al-Hanbali, H., Arnold, E., Backman, J., Mörth, M., 2000. Manganese and color cycles in Arctic Ocean sediments constrain Pleistocene chronology. Geology 28, 23. https://doi.org/10.1130/0091-7613(2000)28<23:MACCIA>2.0.CO;2.

Jakobsson, M., Løvlie, R., Arnold, E.M., Backman, J., Polyak, L., Knutsen, J.-O., Musatov, E., 2001. Pleistocene stratigraphy and paleoenvironmental variation from Lomonosov Ridge sediments, central Arctic Ocean. Glob. Planet. Change 31, 1–22. https://doi.org/10.1016/S0921-8181(01)00110-2.

Jakobsson, M., Nilsson, J., Anderson, L., Backman, J., Björk, G., Cronin, T.M., Kirchner, N., Koshurnikov, A., Mayer, L., Noormets, R., O'Regan, M., Stranne, C., Ananiev, R., Barrientos Macho, N., Cherniykh, D., Coxall, H., Eriksson, B., Flodén, T., Gemery, L., Gustafsson, Ö., Jerram, K., Johansson, C., Khortov, A., Mohammad, R., Semiletov, I., 2016. Evidence for an ice shelf covering the central Arctic Ocean during the penultimate glaciation. Nat. Commun. 7, 10365 https://doi.org/10.1038/ncomms10365.

Kaufman, D.S., Polyak, L., Adler, R., Channell, J.E.T., Xuan, C., 2008. Dating late Quaternary planktonic foraminifer *Neogloboquadrina pachyderma* from the Arctic Ocean using amino acid racemization: amino acid dating Arctic Ocean forams. Paleoceanography 23. https://doi.org/10.1029/2008PA001618.

Knies, J., Matthiessen, J., Vogt, C., Laberg, J.S., Hjelstuen, B.O., Smelror, M., Larsen, E., Andreassen, K., Eidvin, T., Vorren, T.O., 2009. The Plio-Pleistocene glaciation of the Barents Sea–Svalbard region: a new model based on revised chronostratigraphy. Quat. Sci. Rev. 28, 812–829. https://doi.org/10.1016/j.quascirev.2008.12.002.

Lisiecki, L.E., Raymo, M.E., 2005. A Pliocene-Pleistocene stack of 57 globally distributed benthic δ^{18}O records: pliocene-pleistocene benthic stack. Paleoceanography 20. https://doi.org/10.1029/2004PA001071.

Martini, E., 1971. Standard Tertiary and Quaternary calcareous nannoplankton zonation. In: Proceedings of the Second International Conference on Planktonic Microfossils Roma, Rome, pp. 739–785.

Not, C., Hillaire-Marcel, C., 2012. Enhanced sea-Ice export from the arctic during the younger dryas. Nat. Commun. 3, 647. https://doi.org/10.1038/ncomms1658.

Okada, H., Bukry, D., 1980. Supplementary modification and introduction of code numbers to the low-latitude coccolith biostratigraphic zonation (Bukry, 1973; 1975). Mar. Micropaleontol. 5, 321–325. https://doi.org/10.1016/0377-8398(80)90016-X.

O'Regan, M., Backman, J., Fornaciari, E., Jakobsson, M., West, G., 2020. Calcareous nannofossils anchor chronologies for Arctic Ocean sediments back to 500 ka. Geology 48, 1115–1119. https://doi.org/10.1130/G47479.1.

O'Regan, M., Coxall, H.K., Cronin, T.M., Gyllencreutz, R., Jakobsson, M., Kaboth, S., Löwemark, L., Wiers, S., West, G., 2019. Stratigraphic occurrences of sub-polar planktic foraminifera in Pleistocene sediments on the Lomonosov Ridge, Arctic Ocean. Front. Earth Sci. 7, 71. https://doi.org/10.3389/feart.2019.00071.

O'Regan, M., Cronin, T.M., Reilly, B., Alstrup, A.K.O., Gemery, L., Golub, A., Mayer, L.A., Morlighem, M., Moros, M., Munk, O.L., Nilsson, J., Pearce, C., Detlef, H., Stranne, C., Vermassen, F., West, G., Jakobsson, M., 2021. The Holocene dynamics of Ryder Glacier and ice tongue in north Greenland. Cryosphere 15, 4073–4097. https://doi.org/10.5194/tc-15-4073-2021.

O'Regan, M., John, K.St, Moran, K., Backman, J., King, J., Haley, B.A., Jakobsson, M., Frank, M., Röhl, U., 2010. Plio-Pleistocene trends in ice rafted debris on the Lomonosov Ridge. Quat. Int. 219, 168–176. https://doi.org/10.1016/j.quaint.2009.08.010.

O'Regan, M., King, J., Backman, J., Jakobsson, M., Pälike, H., Moran, K., Heil, C., Sakamoto, T., Cronin, T.M., Jordan, R.W., 2008. Constraints on the Pleistocene chronology of sediments from the Lomonosov Ridge: lomonosov RIDGE pleistocene stratigraphy. Paleoceanography 23. https://doi.org/10.1029/2007PA001551.

O'Regan, M., Sellén, E., Jakobsson, M., 2014. Middle to late Quaternary grain size variations and sea-ice rafting on the Lomonosov Ridge. Polar Res. 33, 23672 https://doi.org/10.3402/polar.v33.23672.

Persico, D., Wise, S.W., Jiang, S., 2003. Oligocene-holocene calcareous nannofossil biostratigraphy and diagenetic etch patterns on quaternary placoliths at ODP site 1139 on skiff bank, northern kerguelen plateau. In: Frey, F.A., Coffin, M.F., Wallace, P.J., Quilty, P.G. (Eds.), Proceedings of the Ocean Drilling Program, Scientific Results.

Pirini Radrizzani, C., Castradori, D., Erba, E., Guasti, G., Rizzi, A., 1990. A revised method for observing the same nannofossils specimens with scanning electron microscope and light microscope. Riv. Ital. Paleontol. 95, 449–454.

Polyak, L., Best, K.M., Crawford, K.A., Council, E.A., St-Onge, G., 2013. Quaternary history of sea ice in the western Arctic Ocean based on foraminifera. Quat. Sci. Rev. 79, 145–156. https://doi.org/10.1016/j.quascirev.2012.12.018.

Polyak, L., Bischof, J., Ortiz, J.D., Darby, D.A., Channell, J.E.T., Xuan, C., Kaufman, D.S., Løvlie, R., Schneider, D.A., Eberl, D.D., Adler, R.E., Council, E.A., 2009. Late Quaternary stratigraphy and sedimentation patterns in the western Arctic Ocean. Glob. Planet. Change 68, 5–17. https://doi.org/10.1016/j.gloplacha.2009.03.014.

Purcell, K., Hillaire-Marcel, C., de Vernal, A., Ghaleb, B., Stein, R., 2022. Potential and limitation of 230Th-excess as a chronostratigraphic tool for late Quaternary Arctic Ocean sediment studies: an example from the Southern Lomonosov Ridge. Mar. Geol. 448, 106802 https://doi.org/10.1016/j.margeo.2022.106802.

Raffi, I., Backman, J., Fornaciari, E., Pälike, H., Rio, D., Lourens, L., Hilgen, F., 2006. A review of calcareous nannofossil astrobiochronology encompassing the past 25 million years. Quat. Sci. Rev. 25, 3113–3137. https://doi.org/10.1016/j.quascirev.2006.07.007.

Railsback, L.B., Brook, G.A., Ellwood, B.B., Liang, F., Cheng, H., Edwards, R.L., 2015a. A record of wet glacial stages and dry interglacial stages over the last 560 kyr from a standing massive stalagmite in Carlsbad Cavern, New Mexico, USA. Palaeogeogr. Palaeoclimatol. Palaeoecol. 438, 256–266. https://doi.org/10.1016/j.palaeo.2015.08.010.

Railsback, L.B., Gibbard, P.L., Head, M.J., Voarintsoa, N.R.G., Toucanne, S., 2015b. An optimized scheme of lettered marine isotope substages for the last 1.0 million years, and the climatostratigraphic nature of isotope stages and substages. Quat. Sci. Rev. 111, 94–106. https://doi.org/10.1016/j.quascirev.2015.01.012.

Sabine-Lamoureux, M.E.J., Eynaud, F., Zaragosi, S., Giraudeau, J., Debret, M., Rossignol-Malaize, L., Charlier, K., Billy, I., Malaize, B., Daynac, J., Marches, E., Garlan, T., 2022. Stratigraphy in the Greenland/Iceland/Norwegian (GIN) seas: a multiproxy approach on Pleistocene sediments. In: Stratigraphy & Timescales. Elsevier, pp. 37–80. https://doi.org/10.1016/bs.sats.2022.09.004.

Sato, T., Kameo, K., 1996. Pliocene to Quaternary calcareous nannofossil biostratigraphy of the Arctic Ocean, with reference to late Pliocene glaciation. In: Thiede, J., Myhre, A.M., Firth, J.V., Johnson, G.L., Ruddiman, W.F. (Eds.), Proc. ODP, Sci. Results, 151. TX (Ocean Drilling Program). https://doi.org/10.2973/odp.proc.sr.151.112. Coll. Stn. 39–59.

Sellén, E., O'Regan, M., Jakobsson, M., 2010. Spatial and temporal Arctic Ocean depositional regimes: a key to the evolution of ice drift and current patterns. Quat. Sci. Rev. 29, 3644–3664. https://doi.org/10.1016/j.quascirev.2010.06.005.

Soltwedel, T., Hasemann, C., Vedenin, A., Bergmann, M., Taylor, J., Krauß, F., 2019. Bioturbation rates in the deep Fram Strait: results from in situ experiments at the arctic LTER observatory HAUSGARTEN. J. Exp. Mar. Biol. Ecol. 511, 1–9. https://doi.org/10.1016/j.jembe.2018.11.001.

Song, T., Hillaire-Marcel, C., de Vernal, A., Liu, Y., 2023a. A resilient ice cover over the southernmost Mendeleev Ridge during the late Quaternary. Boreas bor. 12632 https://doi.org/10.1111/bor.12632.

Song, T., Hillaire-Marcel, C., Liu, Y., Ghaleb, B., de Vernal, A., 2023b. Cycling and behavior of 230Th in the Arctic Ocean: insights from sedimentary archives. Earth Sci. Rev. 244, 104514 https://doi.org/10.1016/j.earscirev.2023.104514.

Spielhagen, R., Baumann, K.H., Erlenkeuser, H., Nowaczyk, N.R., Nørgaard-Pedersen, N., Vogt, C., Weiel, D., 2004. Arctic Ocean deep-sea record of northern Eurasian ice sheet history. Quat. Sci. Rev. 23, 1455–1483. https://doi.org/10.1016/j.quascirev.2003.12.015.

Spielhagen, R.F., Bonani, G., Eisenhauer, A., Frank, M., Frederichs, T., Kassens, H., Kubik, P.W., Mangini, A., Nøgaard Pedersen, N., Nowaczyk, N.R., Schaper, S., Stein, R., Thiede, J., Tiedemann, R., Wahsner, M., 1997. Arctic Ocean evidence for Late Quaternary initiation of northern Eurasian ice sheets. Geology 25 (9), 783–786. https://doi.org/10.1130/0091-7613(1997)025<0783:AOEFLQ>2.3.CO;2.

Stein, R., 2015. The expedition PS87 of the Research Vessel Polarstern to the Arctic Ocean in 2014, Berichte zur Polar- und Meeresforschung = Reports on Polar and Marine Research. Alfred-Wegener-Institut, Helmholtz-Zentrum für Polar- und Meeresforschung. https://doi.org/10.2312/BZPM_0688_2015.

Stein, R., Matthiessen, J., Niessen, F., Krylov, A., Sung, N., Bazhenova, E., 2010. Towards a better (litho-) stratigraphy and reconstruction of quaternary paleoenvironment in the Amerasian Basin (Arctic Ocean). Polarforschung 97–121.

Thierstein, H.R., Geitzenauer, K.R., Molfino, B., Shackleton, N.J., 1977. Global synchroneity of late Quaternary coccolith datum levels Validation by oxygen isotopes. Geology 5, 400. https://doi.org/10.1130/0091-7613(1977)5<400:GSOLQC>2.0.CO;2.

Vermassen, F., O'Regan, M., de Boer, A., Schenk, F., Razmjooei, M., West, G., Cronin, T.M., Jakobsson, M., Coxall, H.K., 2023. A seasonally ice-free Arctic Ocean during the last interglacial. Nat. Geosci. 16, 723–729. https://doi.org/10.1038/s41561-023-01227-x.

Vermassen, F., O'Regan, M., West, G., Cronin, T.M., Coxall, H.K., 2021. Testing the stratigraphic consistency of Pleistocene microfossil bioevents identified on the Alpha and Lomonosov Ridges. Arctic Ocean. Arct. Antarct. Alp. Res. 53, 309–323. https://doi.org/10.1080/15230430.2021.1988356.

Wade, B.S., Pearson, P.N., Berggren, W.A., Pälike, H., 2011. Review and revision of Cenozoic tropical planktonic foraminiferal biostratigraphy and calibration to the geomagnetic polarity and astronomical time scale. Earth Sci. Rev. 104, 111–142. https://doi.org/10.1016/j.earscirev.2010.09.003.

West, G., Kaufman, D.S., Jakobsson, M., O'Regan, M., 2022. Amino acid racemization in Neogloboquadrina pachyderma and Cibicidoides wuellerstorfi from the Arctic Ocean and its implications for age models (preprint). Amino acid racemization. https://doi.org/10.5194/gchron-2022-25.

Wollenburg, J.E., Matthiessen, J., Vogt, C., Nehrke, G., Grotheer, H., Wilhelms-Dick, D., Geibert, W., Mollenhauer, G., 2023. Omnipresent authigenic calcite distorts Arctic

radiocarbon chronology. Commun. Earth Environ. 4, 136. https://doi.org/10.1038/s43247-023-00802-9.

Xiao, W., Polyak, L., Wang, R., Not, C., Dong, L., Liu, Y., Ma, T., Zhang, T., 2021. A sedimentary record from the Makarov Basin, Arctic Ocean, reveals changing middle to Late Pleistocene glaciation patterns. Quat. Sci. Rev. 270, 107176 https://doi.org/10.1016/j.quascirev.2021.107176.

Young, J.R., 1998. Neogene nannofossils. In: Bown, P. (Ed.), Calcareous Nannofossil Biostratigraphy. British Micropalaeontology Society Publications Series, Cambridge: Kluwer Academic Publisher, pp. 225–265.